MEASUREMENT OF MATERIAL Q IN RAYLEIGH WAVES WITH A LASER BASED ACOUSTIC SPECTROMETER

A Thesis
Presented to
The Academic Faculty

by

Eric W. Massey

In Partial Fulfillment
of the Requirements for the Degree
Masters of Science in Electrical and Computer Engineering in the
School of Electrical and Computer Engineering

Georgia Institute of Technology
December 2006

MEASUREMENT OF MATERIAL Q IN RAYLEIGH WAVES WITH A LASER BASED ACOUSTIC SPECTROMETER

Approved by:

Dr. William D. Hunt Advisor
School of Electrical and Computer Engineering
Georgia Institute of Technology

Dr. Ali Adibi
School of Electrical and Computer Engineering
Georgia Institute of Technology

Dr. Steve J. Kenney
School of Electrical and Computer Engineering
Georgia Institute of Technology

Date Approved: November 20, 2006

ACKNOWLEDGEMENTS

I would first like to begin by thanking my advisor Dr. Bill Hunt for giving me the opportunity to join the MAG lab and have the pleasure to work with some of the finest students I have met during my 5+ years at Georgia Tech. I am grateful for his guidance on this thesis as well as the input he has always been willing to provide for life in general. I have also thoroughly enjoyed his unique sense of humor which has made this experience much more entertaining. I would also like to thank Dr. Ali Adibi and Saeed Mohammadi for their assistance with the laser probe and general suggestions regarding my work. Their assistance has been invaluable to me. I want to thank Dr. Larry Jacobs for the discussions we had and for introducing me to the acoustic Kramers-Kronig relations. I also want to thank James Steinberg in the senior design lab for helping me with some of my questions during the assembly and modification phases of the laser probe. I also want to express my appreciation for Dr. Steve Kenney for being on my thesis committee. Lastly, I would like to thank Dr. Alex Maznev and Yun Li of Phillips AMS for their donation of the laser probe to our lab and for their assistance along the way.

To the guys in the MAG lab (past and present)[1], it has truly been an honor to work with all of you. I have enjoyed getting to know you and consider you all my friends as well as coworkers. From science and engineering, to politics and religion, to landing on the moon or not landing on the moon, the discussions we have had together have been

---

[1] Ryan Westafer, Tony Dickherber, Chris Corso, Farasat Munir, John Perng, Adam Wathen, George Yu, Dr. "Sangstrom" Lee, and Dr. Desmond Stubbs

some of the most stimulating and entertaining I have had while at Tech. I would also like to thank Ryan Westafer individually for being a fantastic partner in our endeavors to bring the laser probe online.

To my family, friends, and teammates, not already mentioned above, your support has been tremendous and my sanity would not still be intact with out all of you. I want to thank Coach Bradd and Coach Hinsdale for not only giving me the opportunity to compete on the track and field team, but also for giving me the flexibility to pursue my academic goals as well. I would also like to thank my teammates, especially the throwers, who I spent a part of every day with for the past two seasons for their support and frequent entertainment. You guys are all very talented and I look forward to seeing you all dominate the ACC conference. To my many friends I have made at Tech, thank you for being a part of my life and rest assured I would go to bat for any and all of you any day of the week. I would especially like to thank Kelsey and Tomasz for putting up with me as a roommate for the past 5 years and Adrianne for her constant support. Lastly, I want to thank Mom, Dad, Diana, and the rest of my family for their love and support.

TABLE OF CONTENTS

LIST OF TABLES

LIST OF FIGURES

LIST OF SYMBOLS AND ABBREVIATIONS

MAG	Microelectronic Acoustics Group
CAN	Controller Area Network
FDTD	Finite-Difference Tim-Domain
Phillips AMS	Phillips Advanced Metrology Systems

SUMMARY

I have developed a method which can quickly measure the Rayleigh wave Q for a test material using a minimally invasive laser probe. The probe was donated to our lab by Dr. Alex Maznev at Phillips AMS in Natick, Ma. The machine was originally used to measure ultra thin film metal thicknesses; however we have utilized it to suit our needs. The optics head relies on a technique known as the transient grating method to generate a dispersion curve. This dispersion curve is then operated on by a local approximation for the Kramers-Kronig relations. The Kramers-Kronig relations for acoustic waves relate the real and imaginary parts of the dynamic compressibility to one another. The real part of the compressibility relates to the phase velocity of the wave and the imaginary part relates to the attenuation. Once the attenuation for the corresponding range of frequencies is determined the last step is to apply both the dispersion data and the attenuation data to the material Q equation to find Q over a range of frequencies. My thesis discusses the design of the machine, the theory behind the Kramers-Kronig relations and surface acoustic waves, the experimental procedure, and lastly results generated by the technique.

CHAPTER 1

INTRODUCTION

Many RF filters, biosensors, and other microelectronic devices rely on surface acoustic waves for operation. Surface acoustic wave resonators especially rely on one figure of merit, Material Q. Material Q is the ratio of energy stored per cycle divided by energy lost per cycle as the acoustic wave propagates within the medium. The higher the Material Q, the higher the upper limit for the total Q of a resonator or other such acoustic wave device.

There is limited information available for material Q values of Rayleigh waves in literature and in texts. The motivation of this thesis is to be able to rapidly measure the material Q of a given substrate, using minimally invasive techniques. In less than one minute the material Q of a solid can be measured without the need for an IDT to be fabricated on the surface. This thesis describes a novel method we have developed in order to measure material Q based on just the dispersion data. This is done by applying the Kramers-Kronig relationship to the dispersion data over frequency and calculating the corresponding attenuation. Typically in the study of acoustics and geology, attenuation data is first gathered and the Kramers-Kronig relationship is used to calculate the dispersion data. [4, 5] This technique has the added benefit of calculating material Q from one set of data, rather than having to measure the dispersion and attenuation before the calculation can be done.

1.1 Laser Probe Overview

Chapter 3 of this thesis will discuss the details of the laser probe. The laser probe used in the experiment was kindly donated by Alex A. Maznev at Phillips AMS in Natick,

MA. The donated optics head was part of a system called the Impulse 300 which costs in excess of $1,000,000. The optics head and motor stage that was donated to our lab totaled a value in excess of $180,000. The entire system was originally designed for thickness measurements of ultra thin metal films on CMOS circuits. This metrology tool has found much success in the semiconductor industry the measurements were done using a method known as Transient Grating (TG) or Impulsive Stimulated Thermal Scattering (ISTS). A diffraction grating is used to diffract an excitation beam. The two first order diffractions of the beam pass through a set of lenses that recombine the beams at the surface of a test wafer. The angle of recombination dictates the fringe pattern which in turn dictates the wavelength of the acoustic wave generated. The resulting surface acoustic wave is then measured by an IR probe beam which is shone directly on the "ripple" of the surface. The first order diffracted beam is then detected by a high speed avalanche photo receiver and that signal is in turn output to a 2 Gb/s LeCroy Oscilloscope.

The resulting signal can then be analyzed by MATLAB to extract information about the wave. I perform an FFT on the signal to determine the frequency of the propagating wave. The phase velocity of the wave is then calculated using the familiar equation:

$$V_s = \lambda \cdot f \qquad (1.1)$$

where λ is the wavelength of the SAW wave and f is the frequency of the wave. The resultant signal can also be operated on in other ways to provide data useful for calculating material Q for different substances. A detailed description regarding the nature of acoustic waves, more specifically Rayleigh waves will be given in chapter 2.

1.2 Dispersion Data and Kramers-Kronig Calculations

The dispersion curve can be created from the collected velocities at different wavelengths. The dispersion curve is plotted over frequency to view the trend in the change of acoustic phase velocity as the frequency increases. The dispersion data is then operated on by a set of approximations based off the Kramers-Kronig relationship. The Kramers-Kronig relationship was first developed to relate the real and imaginary part of a complex wave number. Essentially, this relationship allows dispersion data to be translated into attenuation data for the corresponding frequencies and vice versa. Unfortunately, advanced knowledge of a point in the destination data set is necessary for the relationship. To mitigate the problem a set of approximations have been developed to allow for dispersion data that is relatively constant over a small range of frequencies to be used to find the corresponding attenuation data. [5, 6]

After the dispersion data is gathered and the corresponding attenuation data has been calculated material Q can be calculated for the corresponding range of frequencies. The formula used for the final calculation of Q is:

$$Q = \frac{\omega}{2 \cdot \alpha \cdot V_a} \qquad (1.2)$$

where ω is the angular frequency, α is the attenuation coefficient and V_a is the velocity of the acoustic wave. [3] Further discussion regarding material Q will be held in chapter 2. A derivation of the Kramers-Kronig relations as well as the approximations used in this experiment will be presented in Chapter 4.

1.3 Experimental Procedure

The fifth chapter will detail the steps needed to perform the experiment. First, the preliminary preparations including wafer preparation, setting up the laser probe, properly aligning the system and other steps will be discussed. Second, the actual control of the machine and operation of the system will be discussed. Last, a description of the Labview based dispersion curve program and the MATLAB mathematical analysis software will both be presented to better explain the code.

CHAPTER 2

BACKGROUND ON SURFACE ACOUSTIC WAVES IN SOLIDS

This chapter will provide the necessary background information regarding surface acoustic waves in solids. This chapter is relevant to this thesis because the acoustic waves generated by the laser probe are surface modes. This chapter will focus on the physics of first order surface waves, known as Rayleigh waves, since they are the waves of study in this thesis. Higher order modes, such as Sezawa modes, can be generated by the laser probe when a thick enough surface layer is present. In my experiment however, the top layer is kept acoustically thin enough that these modes are not present.

This section will be divided into two parts, the first discussing Rayleigh Wave physics and propagation, the next discussing material Q for acoustic waves, primarily Rayleigh waves. Discovered in 1887 by Lord Rayleigh, Rayleigh waves are surface acoustic waves that are confined to the surface of a medium. The energy of the wave decays exponentially into the substrate and is typically non existent at a depth on the order of a wavelength. Material Q for Rayleigh waves is an important figure of merit since it is a necessary parameter used by engineers when designing acoustic devices.

2.1 Rayleigh Wave Background

A subset of all surface acoustic wave polarizations, the Rayleigh wave is a common mode seen anywhere from resonators and sensors, to earthquakes traveling along the earth’s surface. A Rayleigh wave has an elliptical polarization where the center of the rotation is located along the y-axis as seen in figure 2.1.

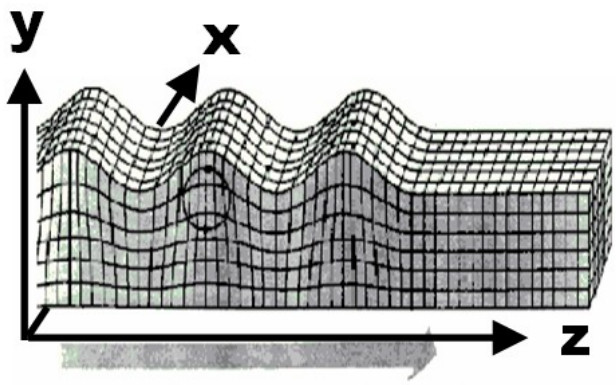

Figure 2.1. Elliptical Polarization of Rayleigh Waves [1]

Ocean waves are similar to Rayleigh waves with the exception of the polarization of the elliptical particle displacement. While Rayleigh waves are polarized in the counterclockwise rotation, ocean waves posses a clockwise rotation and ultimately result in a different wave profile as seen in figure 2.2. The elliptical shape of the polarization is due to the fact that the air has lower impedance than the solid. This results in more displacement along the direction normal to the surface. [2]

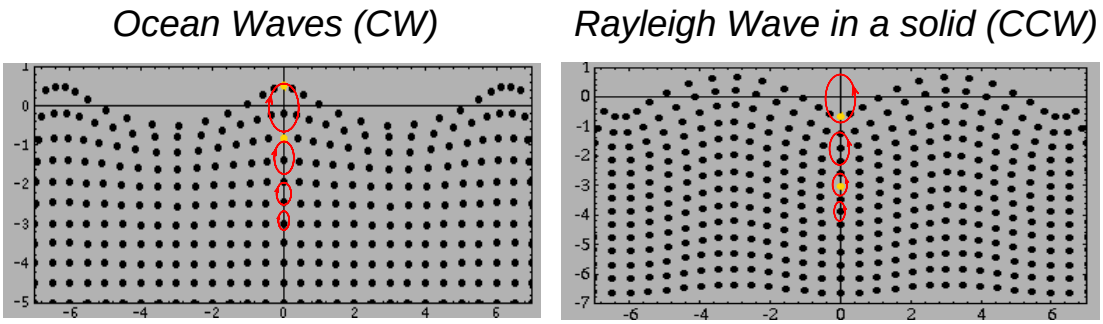

Figure 2.2. Profile of Ocean Waves versus Rayleigh Waves

The Rayleigh Wave itself is actually a combination of a longitudinal mode and a shear transverse mode propagating on an infinite substrate. If the substrate is not considered infinite, a Lamb Wave can develop. A lamb wave occurs when the energy

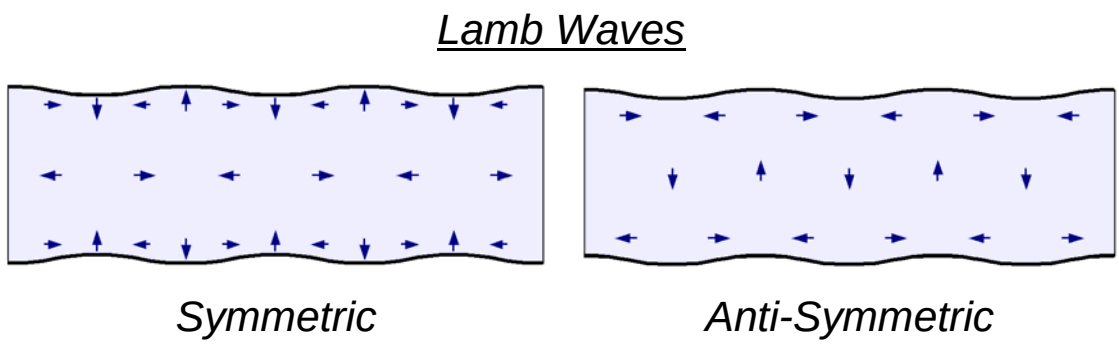

Figure 2.3. Symmetric versus Anti-Symmetric Lamb Waves

from a Rayleigh Wave on one side of a substrate couples to the other side creating symmetric or anti-symmetric propagating waves (figure 2.3). For the experiments in this thesis the substrate is considered infinite because the thickness (~500 um) is an order of magnitude greater than the length of the acoustic wavelength (~10 um).

The characteristic equation used to relate the velocities of the longitudinal and shear components of a Rayleigh wave takes the form:

$$\left(\frac{V_R}{V_s}\right)^6 - 8\left(\frac{V_R}{V_s}\right)^4 + 8\left\{3 - 2\left(\frac{V_s}{V_l}\right)^2\right\}\left(\frac{V_R}{V_s}\right)^2 - 16\left\{1 - \left(\frac{V_s}{V_l}\right)^2\right\} = 0 \qquad (2.1)$$

where V_s and V_l are the longitudinal and shear component velocities and V_R represents the Rayleigh velocity. V_R takes the form:

$$V_R = \frac{\omega}{\beta_R} \qquad (2.2)$$

The solution for $\frac{V_R}{V_s}$ must be real and positive and therefore only one solution exists. Figure 2.4 gives the solution as a function of the shear and longitudinal velocities in the substrate. This solution can also be approximated by using the formula:

$$\frac{V_R}{V_s} = \frac{0.87 + 1.12\sigma}{1+\sigma} \quad (2.3), \qquad \text{where } \sigma = \frac{1 - 2\left(\frac{V_s}{V_l}\right)^2}{2\left(1 - \left[\frac{V_s}{V_l}\right]^2\right)} \quad (2.4)$$

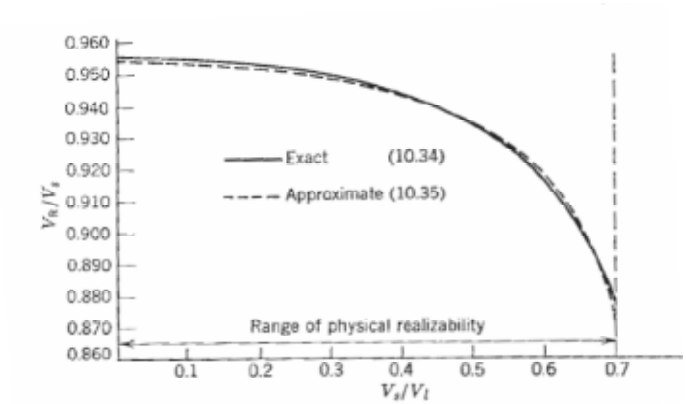

Figure 2.4. Exact versus approximate solution to the Rayleigh wave characteristic equation[2]

This figure shows how good of an approximation equation 2.3 is for estimating the solution to the Rayleigh wave characteristic equation. [2]

The field pattern for Rayleigh waves is shown in figure 2.5 below and clearly demonstrates how the energy of the wave decays going into the bulk. The partial velocity field is a combination of the longitudinal field partial wave and the shear field partial wave. The two partial wave velocity field patterns follow the equations:

$$v_y = \mp i\beta_R \left\{ e^{-\alpha t_s y} - \frac{2\alpha_{tl}\alpha_{ts}}{\beta_R^2 + \alpha_{ts}^2} e^{-\alpha_{tl} y} \right\} e^{\mp i\beta_R z} \qquad (2.4)$$

$$v_z = \alpha_{ts} \left\{ e^{-\alpha t_s y} - \frac{2\beta_R^2}{\beta_R^2 + \alpha_{ts}^2} e^{-\alpha_{tl} y} \right\} e^{\mp i\beta_R z} \qquad (2.5)$$

The particle displacement field distribution is elliptically polarized in the *yz* plane. Near the surface the Rayleigh wave motion is retrograde yet it reverses its sense at roughly a fifth of a wavelength into the bulk. Along with the varying polarization, the aspect ratio of the elliptical polarization varies with depth. [2]

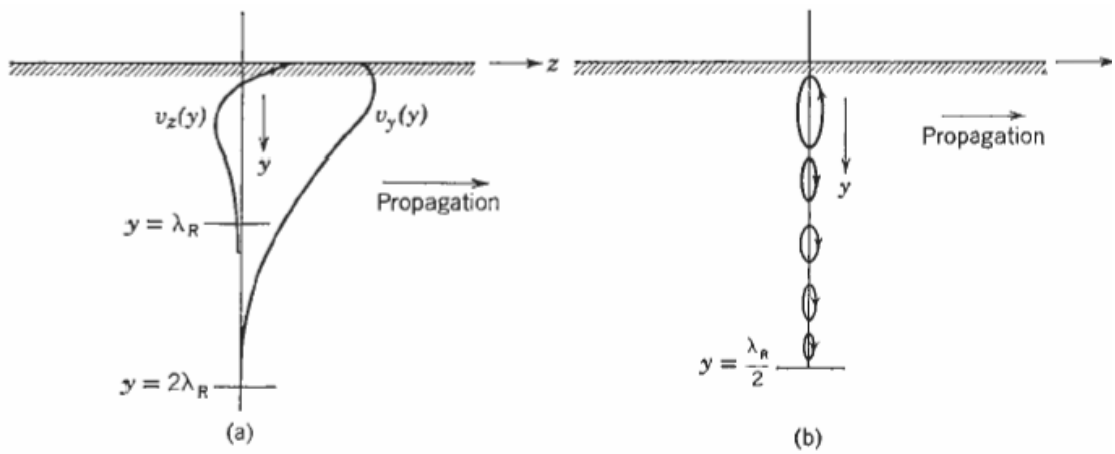

Figure 2.5. (a) Particle velocity field distribution, (b) Particle displacement field distribution [2]

2.2 Material Q Background

In general the quality factor is a figure of merit which attempts to measure the amount of energy saved per cycle divided by the amount of energy lost per cycle. This figure of merit is used across all fields of wave theory. Acoustic waves, like all waves, simply do not propagate with out any loss to the signal. If this were the case then Hooke's Law (T = CS) would be a precise equation requiring no modification for advanced calculations. Unfortunately, this is not the case due to viscous damping forces and nonlinearities within a solid and as a result Hooke's Law must be compensated to account for this. Equation 2.6 accounts for loss due to viscosity in Hooke's Law.

$$T = CS + \eta \frac{dS}{dt} \qquad (2.6)$$

Viscosity is represented by η and has units of N s/m^2. The time derivative in the equation is due to the relaxation of strain as it settles toward equilibrium. [3]

The imperfect propagation of acoustic waves due to these damping forces and nonlinearities within the medium is measured by absorption. Absorption is the amount of energy lost versus the distance the wave has traveled. Derived in Rosenbaum [3] using the wave equation in 2.7 and complex wave number (equation 2.8), the expression for absorption takes the form seen in equation 2.9.

$$\rho \frac{\partial^2 v}{\partial t^2} = C \frac{\partial^2 v}{\partial z^2} + \eta \frac{\partial^3 v}{\partial t \partial z^2}, \qquad (2.7)$$

$$\hat{k} = \frac{\omega}{v_a} + j\alpha, \qquad (2.8)$$

$$\alpha = \frac{\omega\eta}{v_a^2 \rho}\left(\frac{\omega}{2v_a}\right) = \frac{\omega}{2Qv_a}, \qquad (2.9)$$

In the above equations C is the stiffness constant, ρ is the density of the material, η is the viscosity of the material, and Q represents the material quality factor.

Material Q itself is defined as the ratio of the amount of energy stored versus the amount of energy lost per cycle [4]. More specifically the value for material Q can be calculated using the absorption coefficient, velocity, and frequency in equation 2.9.

$$Q = \frac{\omega}{2\alpha v_a} \qquad (2.9)$$

Material Q varies over frequency and for homogenous material tends to be inversely proportional to frequency. This is because the absorption coefficient is proportional to the frequency squared. Typically in practice, the frequency dependence is ω^n, where 1.2 < n

< 1.4 for poor quality materials and n > 1.8 for high quality materials. When n < 1.7 one can expect reduced absorption if the crystal growth conditions are improved. For heterogeneously layered materials the slope of the Q factor is less predictable as frequency changes. For anisotropic media material Q can also vary but usually no more than 5% to 10% over direction, however a notable exception to this is paratellurite (TeO_2) where the Q value can vary over orders of magnitude. [3]

In the case of acoustic resonators, material Q serves as the upper bound for the potential value of the resonator Q [7].This means it is very important to know the material Q of the design materials ahead of time to ensure the resonator can be built with at least a certain Q value. I will now derive the equation for total resonator Q. To do so, the generalized definition for Q must be revisited. Equation 2.10 represents the energy lost divided by energy stored per cycle, where ω_0 is the frequency of the wave, E_s is the energy stored, and P_L is the energy loss rate.

$$Q = \frac{\omega_0 E_s}{P_L} \qquad (2.10)$$

The first step in the derivation begins with considering all the different energy losses, including the loss due to the material, and losses due to the efficiency of the resonator in an ideal situation.

$$Q_{Total} = \frac{\omega_0 E_s}{\left(P_{LMaterial} + P_{L\,\mathrm{Re}\,sonator} + \cdots + P_{LN}\right)} \qquad (2.11)$$

By taking the inverse of both sides of the equation as in 2.12 and 2.13 it becomes possible to split each energy loss into its own term.

$$\frac{1}{Q_{Total}} = \frac{\left(P_{LMaterial} + P_{L\,\mathrm{Re}\,sonator} + \cdots + P_{LN}\right)}{\omega_0 E_s} \qquad (2.12)$$

$$\frac{1}{Q_{Total}} = \frac{P_{LMaterial}}{\omega_0 E_s} + \frac{P_{L\,\mathrm{Re}\,sonator}}{\omega_0 E_s} + \cdots + \frac{P_{LN}}{\omega_0 E_s} \qquad (2.13)$$

Once each term is alone it becomes clear that each energy loss term is simply the inverse value for Q. Equation 2.14 accounts for not only the material and resonator Q values but any other loss mechanisms that may be accounted for within the system.

$$\frac{1}{Q_{Total}} = \frac{1}{Q_{Material}} + \frac{1}{Q_{\mathrm{Re}\,sonator}} + \cdots + \frac{1}{Q_N} \qquad (2.14)$$

Much like the equation for adding parallel resistive terms in electronic circuitry, the smallest Q value in the system dominates the total value for Q. Conversely, larger Q values tend to have less of an affect on the overall Q for the system. As a result of this, whenever the material Q is large in comparison to the other aspects of the system it plays a minor role in affecting the total Q value. If the material Q value is the smallest amongst the other Q values in the system it then dominates the entire system and the total Q can never be anything greater than the value of material Q.

CHAPTER 3

THE LASER PROBE

This chapter will go into detail of the laser probe optics head design, the preparatory work done to bring it online, and the underlying physics of operation. The optics head of the laser probe is a very space efficient design and relies completely on transmissive components. The details of this design are discussed in the first section of this chapter. The original commercial laser probe included many features that were not necessary for our application; i.e. wafer handling. This led to only the principle components being donated to our lab including the optics head and the motor stage. The second section of this chapter will discuss the preparations, modifications, and software written we had to do to bring the entire laser probe system online. The last section of this chapter will explain, in detail, the physics behind the laser probe.

3.1 Laser Probe Design

The first version of the metrology tool was built very elegantly with consideration to the space the optical components took up. An image of the optics head is pictured on the left of figure 3.1 and a diagram for the system is pictured on the right side of the figure. This section will be broken down into the subsystems of the laser probe: the excitation beam, the probe beam and receiver, the camera view, and the motor control.

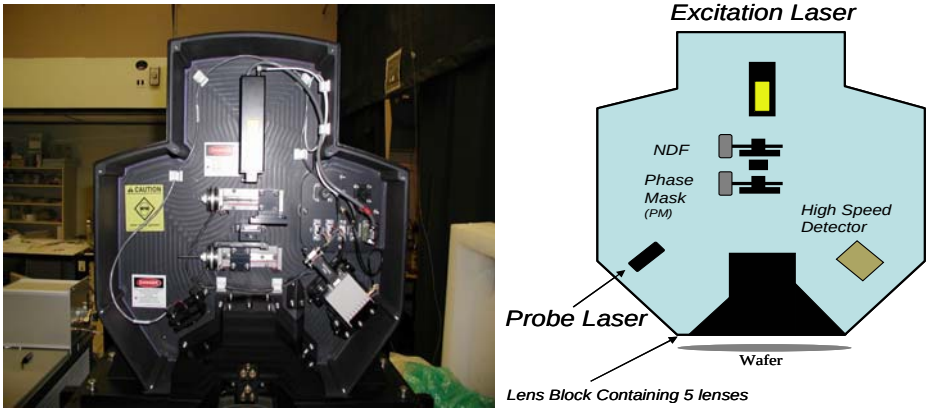

Figure 3.1. The laser probe optics head and corresponding schematic

3.1.1 Excitation Beam

The excitation beam is generated by a ND:YAG laser which creates a beam with a wavelength of 1064 nm. The beam is pulsed with duration of ~100 picoseconds and is passively Q switched at 200 us. A frequency doubler is used on the excitation laser resulting in an actual wavelength of 532 nm. The excitation beam first travels through a neutral density filter in order to control the intensity of the beam on the surface. The attenuated light then passes through a cylindrical lens which elongates the beam. Next the excitation beam passes through a phase mask which diffracts the beam. The two first order diffracted beams are then passed through a set of lenses above the test wafer and refocused on the surface to create an interference pattern. The size of the interference pattern is ~300 microns thick and roughly a millimeter in the direction of the generated acoustic wave. The width of the pattern varies depending on which phase mask is used. Figure 3.2 is a diagram representing the path of the excitation beam through the optics head on the way to the device under test.

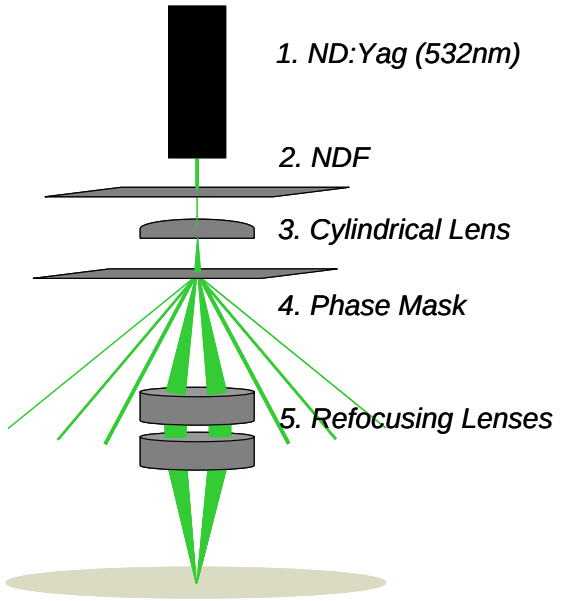

Figure 3.2. The optical path of the excitation beam

3.1.2 Probe Beam

The probe beam consists of a continuous wave AlGaAs IR diode laser with an optical wavelength of 808 nm. The probe beam is directed onto the surface of the device under test at a position incident to the excitation beam pattern. The spot size of the beam on the surface of the sample is roughly 100 microns. The acoustic waves generated by the excitation beam act as a diffraction grating for the IR probe beam. The probe light that is reflected from the surface is directed towards a stop while the diffracted light is aimed at a lens that directs the light toward the high speed detector. The detector utilizes a Silicon avalanche photodiode with a frequency range of 1 MHz up to 1 GHz. The photoreceiver outputs the signal to a LeCroy Oscilloscope which is in turn connected to the desktop computer. The schematic for the optical arrangement is depicted in Figure 3.3.

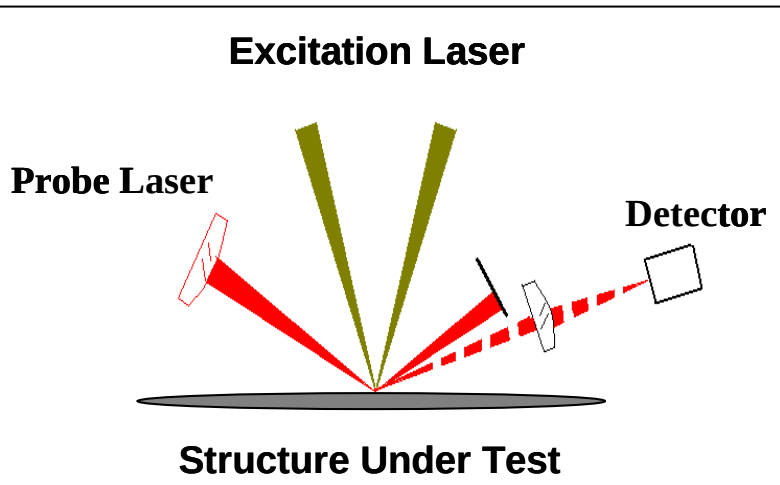

Figure 3.3. The optical path of the probe beam

3.1.3 Motor Control, Laser Control, and Camera View

The stage motor control and the stepper motors in the optics system take full advantage of a CAN Open network. Five total amplifiers are used; three for the XYZ stage, one for the NDF stepper motor and one for the phase mask stepper motor. The

stage motors have a precision to a third of a micron allowing for reliable and precise targeting of the laser. The stepper motors within the optics system allow for fast NDF and phase mask setting changes. Whenever a certain phase mask or NDF setting is selected, the software tells the amplifiers to go to the preset locations. The CAN Open network also assists in the controls of the stage light and laser using a few of the pins on amp 4 that have been configured to act as outputs. The output sends a high signal to the Nanolase power supply which controls the pulsing of the laser.

The CCD camera focus is controlled by the Optem Zoom 100D optics set. Initially the system relied on a motor controlled focus lens set, however to save amplifiers a hand controlled optics Zoom 100D was selected. The image from the CCD is sent to the desktop computer and displayed in the control software.

3.2 Laser Probe Preparation

The components of the system that were donated include the motor stage, the optics head, and the nanolase power supply. The total value of the donated equipment came to $180,000. To bring the system online more components were necessary. Power sources for the nanolase power supply, the photoreceiver, and CCD camera were introduced to the system. This DC power supply came from an old laser based experiment previously done in the MAG lab. Each motor also needed an amplifier to control it. The solution was found using a CAN Open amplifier network. These robust amplifiers are networked together and independently addressed. This allowed for improved simplicity when programming the software to control the system. The amplifiers were directly controlled by a desktop computer purchased solely for the operation of the laser probe.

Another important component for the system that was not donated to our lab was the control software. While this was initially an obstacle in the set up of the laser probe, the flexibility for software adaptation in later experiments came to be a strong advantage of our system. I developed the graphical user interface in LabView 8.0 and designed it to be capable of controlling virtually every aspect of the laser probe. Appendix B includes screen shots the GUI for the laser probe.

In the upper left corner of the interface are the relative position controls. The distance in micro steps are entered into the numeric input and the direction buttons move the stage the input distance in the selected direction. Each micro step corresponds to one third of a micron. Below the relative position controls are the absolute position controls. By entering in the coordinates of each axis and pressing GO, the motor stage will accurately position the laser over that location. Underneath the absolute position control are a few buttons that include control over the stage light, and lasers themselves. Control of the NDF and phase mask motors are done by selecting the position on the sliding index bar. Whenever a new position is selected the green light to the right of the bar comes on and the software will not respond to any other commands until the slide is in position. To the right of these controls is the camera image. The cross hairs in the middle of the image represent the location of the lasers being fired on the device under test. At the bottom of the GUI is the waveform as it is seen on the oscilloscope. The user can download the data from the oscilloscope onto the computer by selecting the “capture waveform” button. If the user wishes to store the downloaded waveform, he can do so but selected the save button next to the waveform.

The slowness curve controls are used to gather velocities over a range of frequencies from isotropic solids. This program relies on the aluminum wafer used to orient wafers over direction discussed in chapter five. To run the program the user must first input the start and finish angles as well as the increment size between angles. Then the software will prompt the user to move the aluminum plate to the correct starting angle. Once completed, the user clicks “OK” for the software to capture a waveform at that orientation. Once the capture is complete, the program prompts the user rotate the plate to the next angle and waits for the user to indicate completion. This cycle continues until all angles have been visited.

The dispersion curve button runs a script that prepares a set of waveforms from the phase masks selected by the array input. For each phase mask selected the laser probe will take a summed average of the waveform for 500 sweeps. After each averaged waveform has been downloaded onto the computer, the software saves all the data in a text file where all the odd columns correspond to the time axis of each waveform and all the even columns correspond to the amplitude axis of each waveform. A more detailed description of this program will be covered in chapter five.

3.3 Laser Probe Theory of Operation

This section will discuss why and how the laser probe works and how to interpret the resultant waveforms. This subsection will be broken into sections describing the optics of the excitation beam, acoustic generation by thermal expansion, and lastly interpretation of the data. The goal of this section is to give a general understanding of how the waves are being generated and measured.

3.3.1 Excitation Beam Optics

The principle optical component of the laser probe itself is the transmissive phase mask along the path of the excitation beam. The purpose of this binary phase mask is to diffract the beam as it passes through the glass. Approximately 80% of the incident light is propagated into the +1 and -1 diffraction orders[8]. The angle of diffraction of the two first order beams diffracted through the phase mask follow the equation below:

$$\sin\theta_i = \sin\theta - i\frac{\lambda}{\Lambda \cdot n} \qquad (3.1)$$

where θ_i represents the angle of diffraction for the ith order, Λ represents the grating spacing, n is the index of refraction of the air around the phase mask and λ is the wavelength of the light[9]. Figure 3.5 is a diagram of the excitation pulse passing through the phase grating.

The angle that the two first order beams are diffracted from the phase mask is equal to the angle at which the two beams recombine on the test surface. Earlier designs of the laser probe relied on a reflective phase mask which took up a great deal more space. The transmissive grating allows for a much more space efficient design because no extra mirrors are necessary to direct the beams.

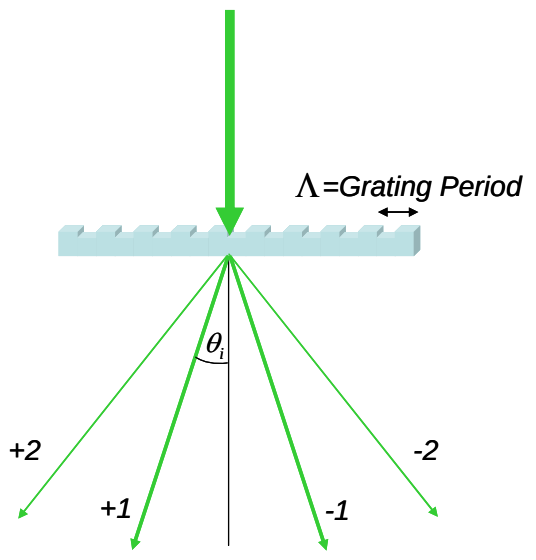

Figure 3.4. Diffracted orders of light after beam passes through a transmissive binary phase mask

3.3.2 Acoustic Wave Generation

As the excitation beam recombines on the surface, an interference pattern is created. The spacing of this pattern follows the equation in 3.2 where Λ is the spatial period of the pattern, λ_e is the excitation wavelength, and θ is the angle of recombination. [8]

$$\Lambda = \frac{\lambda_e}{2 \cdot \sin(\theta / 2)} \qquad (3.2)$$

Figure 3.6 is an example of what the spatial interference pattern looks like on the surface of the target. Provided the surface material has a strong enough emission frequency at the optical frequency of the excitation pulse, the excitation light can be absorbed. This absorption leads to a sudden, spatially periodic heating followed by thermal expansion. This thermal expansion results in the launching of counterpropagating acoustic waves.

The wave vector of these acoustic waves correlates to the spatial wavelength of the interference pattern. The ripple of the acoustic wave acts as a diffraction grating for the probe beam to interact with. The vertical displacement of this ripple due to the thermal absorption at the interference pattern is on the order of 100 nm [10, 11].

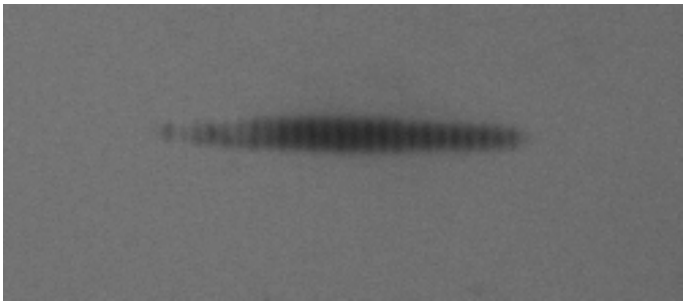

Figure 3.5. A burnt excitation pattern with 8.825 micron spacing

The waveforms acquired by the laser probe measurement technique carry a wealth of information. Along with the acoustic wave data, a low frequency component exists due to the slow decay of the surface displacement associated with the temperature grating. Coupling between the air above the surface of the material and the counterpropagating acoustic waves also create slow oscillations that show up in the resultant signal. The most prominent component of the signal, however, is from the high frequency counterpropagating waves. The two counterpropagating waves alone produce a modulation of the signal that is twice the acoustic frequency. A single acoustic wave, along with the static thermal grating, modulate the probe beam at exactly the frequency of the propagating acoustic wave. As long as the slowly decaying static thermal grating is present in the waveform, the measured acoustic frequency is accurate for the generated wave.[8, 10, 11]

3.3.3 Waveform Analysis

The waveform generated by the laser probe carries a wealth of information that can be analyzed to learn many characteristics of the material. A typical waveform, such as the one seen in figure 3.6, consists of a periodic dampened oscillation after an initial spike from thermal expansion. The decay of the total amplitude of the signal is from the surface displacement of the material over time. The oscillations within the envelope of the signal directly correspond to the frequency of the wave, which can be used to calculate the wave velocity if the wave vector is known. [8, 10, 11]

The ability to rapidly select a different phase mask allows for the generation of multiple waveforms for different acoustic k vectors in a short amount of time. This makes it very easy to create dispersion curves which can later be used for further calculations. By taking the fast Fourier transform of the signal it is easy to extract the frequency. The waveform must be cleaned up to obtain the frequency of the signal. Figure 3.6 shows before and after images of the cleaning process of the waveform.

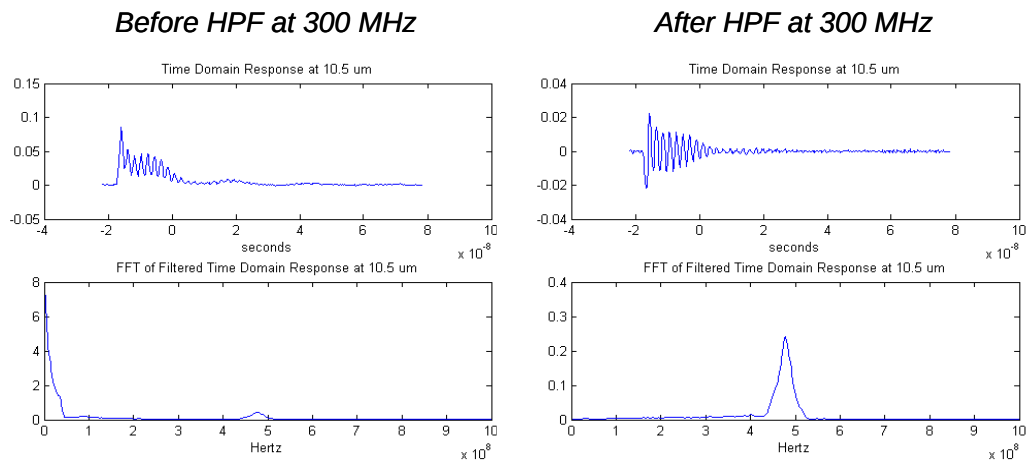

Figure 3.6. Before and after image of a cleaned up waveform generated by a binary phase mask with a spatial period of 10.5 um

It is clear from these diagrams that the low frequency components generated by thermal decay are sufficiently filtered out and the remaining acoustic data can freely be operated on.

CHAPTER 4

KRAMERS-KRONIG RELATIONS

The most essential part for the calculations of this experiment relies on the relationship known as the Kramers-Kronig relations. This relationship was first pioneered in the mid 1920s by Ralph Kronig and Hendrik Anthony Kramers to explain the absorption and dispersion in the X-Ray spectra [12, 13]. In essence, this pair of equations provides the ability to take dispersion data over a range of frequencies and calculate the corresponding set of attenuation data and vice versa. An analogous version to the Kramers-Kronig relationship used to describe optical waves has been developed [5, 6] to explain acoustic waves using the real and imaginary part of the dynamic compressibility. Like the optical counter part, the acoustic version of this relationship requires the system to be both causal and linear.

Much like the original Kramers-Kronig relationship for optical systems, *a priori* information is required in order to translate imaginary or real data to its counterpart. In other words, for a given set of dispersion data to be converted to the attenuation data of the same frequency range, it is necessary to have information about the attenuation data ahead of time. For some applications, such as this experiment, the “anchor point” may not be known and a set of approximations are needed to circumvent the lack of information. The Kramers-Kronig relations are also a nonlocal relationship. In other words, in order for the attenuation to be calculated from the dispersion, the dispersion for all frequencies must be known. The approximations I have used in this thesis also approximate the Kramers-Kronig relationship locally. This section will first discuss the

origin and derivation of the Kramers-Kronig relationship and end with the derivation of the approximations used in this experiment.

4.1 Derivation of the Kramers-Kronig Relations

The original utility of the Kramers-Kronig relations was to relate the imaginary and real parts of the complex permittivity of an electromagnetic wave. This section will derive the Kramers-Kronig relationship based on the derivation found in the second edition of *Semiconductor Optoelectronic Devices* by Pallab Bhattacharya [14]. This derivation will begin with the complex dielectric constant of material for electromagnetic waves where the constant is given by:

$$\in_r(\omega) = \in_r'(\omega) + j \in_r''(\omega) \tag{4.1}$$

In the time-invariant form the electric field **E** and the electric flux density **D** are related by

$$\begin{aligned} \mathbf{D} &= \in_0 (1+\chi^e)\mathbf{E} \\ &= \in_r \in_0 \mathbf{E} \end{aligned} \tag{4.2}$$

where χ^e is the electric *susceptibility*. Any temporal response of **D** due to a change or switching of **E** must include the change of polarization with time. The below expression expresses the causality relationship between the electric field and electric flux density.

$$\mathbf{D}(t) = \in_0 \in_\infty' \delta(t)\mathbf{E}(t) + \int_{-\infty}^{t} \in_0 f(t-t')\mathbf{E}(t')dt' \tag{4.3}$$

This integral represents how the system at time *t* responds to the applied field at **E** at a previous time *t*'. The Fourier transforms for both **D** and **E** are written as

$$\mathbf{D}(t) = \frac{1}{2\pi}\int_{-\infty}^{\infty} \mathbf{D}(\omega)e^{-j\omega t}d\omega \tag{4.4}$$

and

$$\mathbf{E}(t) = \frac{1}{2\pi}\int_{-\infty}^{\infty} \mathbf{E}(\omega) e^{-j\omega t} d\omega \,. \tag{4.5}$$

By substituting the Fourier transforms into the above causality relation one finds

$$\int_{-\infty}^{\infty} \left[\mathbf{D}(\omega) - \in_0 \left(\in'_\infty + f(\omega)\right)\mathbf{E}(\omega)\right] e^{-j\omega t} d\omega \tag{4.6}$$

with

$$f(\omega) = \frac{1}{2\pi}\int_{-\infty}^{\infty} f(t) e^{j\omega t} dt \,. \tag{4.7}$$

Because equation 4.6 must be valid for all values of *t*, the relation

$$\mathbf{D}(\omega) = \in_0 \left(\in'_\infty + f(\omega)\right)\mathbf{E}(\omega) \tag{4.8}$$

is valid between the Fourier components, so that

$$\in_r (\omega) = \in'_\infty + \frac{1}{2\pi}\int_{-\infty}^{\infty} f(t) e^{j\omega t} dt \tag{4.9}$$

$$= \in'_\infty + f(\omega) \tag{4.10}$$

The *Cauchy principle value theorem* can be shown as

$$P\int_{-\infty}^{\infty} \frac{f(\omega')d\omega'}{\omega' - \omega} - j\pi f(\omega) = 0 \tag{4.11}$$

where *P* represents that the principle value of the integral. The second part of the above equation represents the infinitesimally small semi-circle about the simple pole $\omega' = \omega$. The contour integrated over by the *Cauchy principle value theorem* is shown in figure 4.1 From equation 4.11, by application of the Cauchy theorem to the function $\left[\in'_r (\omega) - \in'_\infty\right]/(\omega' - \omega)$, the following relations can be derived.

$$\in'_r (\omega) = \in'_\infty + \frac{2}{\pi} P\int_0^{\infty} \frac{\omega' \in''_r (\omega) d\omega'}{\omega'^2 - \omega^2} \tag{4.12}$$

$$\in_r''(\omega) = -\frac{2}{\pi} P \int_0^{\infty} \frac{[\in_r'(\omega) - \in_\infty']d\omega'}{\omega'^2 - \omega^2} \qquad (4.13)$$

These integrals are the Kramers-Kronig relations for the complex permittivity of material.

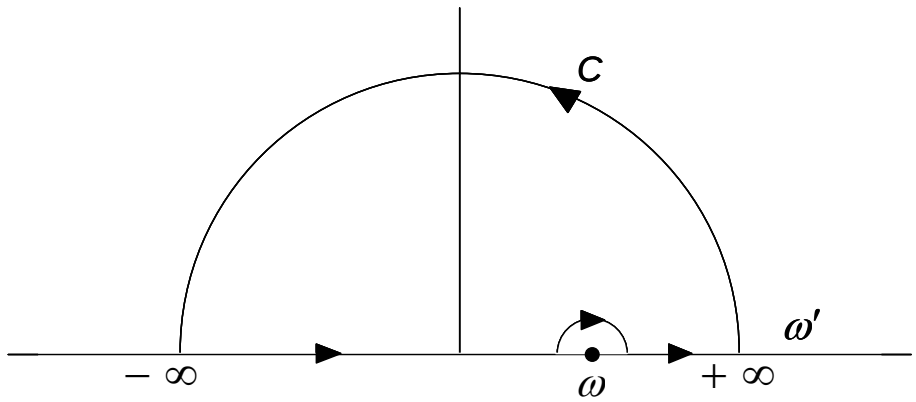

Figure 4.1. The infinite half-circle contour used in the *Cauchy principle value theorem*, with no poles above the real axis [14]

4.2 Derivation of the Kramers-Kronig Approximations for Acoustic Applications

Acoustic wave theory and optical wave theory are analogous in the governing equations. Figure 4.2 compares the one-dimensional acoustic equations to Maxwell's equations for both the fundamental physical laws and the constitutive relations.

One-Dimensional Acoustic Equations	*Maxwell Equations*
FUNDAMENTAL PHYSICAL LAWS	
$\frac{\partial T}{\partial z} = \rho \frac{\partial v}{\partial t}$ Newton's law	$\nabla \times \mathbf{E} = -\frac{\partial \mathbf{B}}{\partial t}$ Faraday's law
$S = \frac{\partial u}{\partial z}$	$\nabla \times \mathbf{H} = \frac{\partial \mathbf{D}}{\partial t} + \mathbf{J}$ Ampere's law
CONSTITUTIVE EQUATIONS	
$T = CS$ Hooke's law	$\mathbf{D} = \epsilon \mathbf{E}$
$v = \frac{\partial u}{\partial t}$	$\mathbf{B} = \mu \mathbf{H}$

Figure 4.2. A comparison between the common acoustic and optical governing equations [3]

From the table it is worth noting how the stiffness constant C is analogous to the electromagnetic permittivity. The compressibility K is the inverse of the stiffness constant. For the Kramers-Kronig relationship for acoustic waves the real and imaginary parts of the compressibility are used and the relationship can be defined as

$$K_1(\omega) = K_1(\infty) + \frac{2}{\pi} P \int_0^\infty \frac{\omega' K_2(\omega')}{\omega'^2 - \omega^2} d\omega' \tag{4.14}$$

$$K_2(\omega) = -\frac{2}{\pi} P \int_0^\infty \frac{\omega K_1(\omega')}{\omega'^2 - \omega^2} d\omega' \tag{4.15}$$

where K_1 and K_2 are the real and imaginary part of the adiabatic compressibility of a medium. This relationship has been verified by various researchers studying the properties of acoustic waves [5, 6, 15]. The remainder of this section will derive the approximation equations used in this experiment; the derivation will come from the M. O'Donnell, E. T. Jaynes, and J. G. Miller paper published in the *Journal for the Acoustical Society of America*[5].

The compressibility of an acoustic wave is related to the wavenumber of that wave by

$$k^2 = \omega^2 \rho_0 K(\omega) \tag{4.16}$$

where k is the wavenumber and ρ_0 is the density of the medium. The complex wavenumber is expressed as

$$\hat{k} = \frac{\omega}{C(\omega)} + j\alpha(\omega) \tag{4.17}$$

where C is the phase velocity and α represents the absorption coefficient. The compressibility can be related to the absorption and phase velocity by substituting equation 4.17 into equation 4.16 yielding

$$\frac{\omega^2}{C^2(\omega)} - \alpha^2(\omega) + \frac{2i\omega\alpha(\omega)}{C(\omega)} = \omega^2\rho_0\left[K_1(\omega) + iK_2(\omega)\right]. \quad (4.18)$$

By separating the imaginary and real components of the previous equation one yields

$$\frac{\omega^2}{C^2(\omega)} - \alpha^2(\omega) = \omega^2\rho_0 K_1(\omega) \quad (4.19)$$

and

$$\frac{2\alpha(\omega)}{C(\omega)} = \omega\rho_0 K_2(\omega). \quad (4.20)$$

These equations decouple for the usual case in which the magnitude of the imaginary part of the wavenumber is much less than the magnitude of the real part [i.e., $\alpha(\omega)C(\omega)/\omega << 1$] for all frequencies. The decoupled equations that relate K_1 with $C(\omega)$, and K_2 with $\alpha(\omega)$ can be written as

$$C(\omega) = 1/\left[\rho_0 K_1(\omega)\right]^{1/2} \quad (4.21)$$

$$\alpha(\omega) = \left[\rho_0 C(\omega)/2\right]\omega K_2(\omega) \quad (4.22)$$

Equations 4.14, 4.15, 4.21, and 4.22 allow for a complete relationship between the attenuation coefficient and phase velocity in the frequency domain. Unfortunately, this relationship is non local since the computation of one variable necessitates knowledge of the complementary variables for all frequencies.

The next part of this derivation will rely on the analogy between the acoustic Kramers-Kronig relation and the relationship between the frequency dependence of the gain and phase shift of an electrical amplifier. This relationship will allow for the derivation of the approximation over a small frequency range in a non resonant system. Bode demonstrated that at any frequency, the phase shift is directly related to the change in amplitude over frequency [16]. Provided the system exhibits no resonances, the

approximation is very accurate over a limited frequency range centered at the frequency of interest. The derivation of this similar approximation for attenuation and phase velocity begins with equation 4.15 and by implementing a change of variable $x = \ln(\omega'/\omega)$ to evaluate the integral. The imaginary part of the compressibility becomes

$$K_2(\omega) = -\frac{2}{\pi}\int_{-\infty}^{\infty} \frac{G(x) - G(\infty)}{e^x - e^{-x}} dx \qquad (4.23)$$

where $G(x) = K_1(\omega')$ and $G(\infty) = K_1(\infty)$ since x is infinite for ω' equal to infinity. Using integration by parts, the imaginary component of compressibility reduces to

$$K_2(\omega) = -\frac{2}{\pi}\int_{-\infty}^{\infty} \frac{dG(x)}{dx} \ln\coth\left(\frac{|x|}{2}\right) dx . \qquad (4.24)$$

From the behavior of the function $\ln\coth(|x|/2)$ seen in figure 4.2 the above equation can be cast into an approximate local form. The sharp singularity around the point x=0 causes the magnitude of the integral to be dominated by the value of x=0. The integral is now rewritten as

$$K_2(\omega) = -\frac{1}{\pi}\int_{-\infty}^{\infty} F(x) \ln\coth\left(\frac{|x|}{2}\right) dx , \qquad (4.25)$$

where $F(x)$ is equal to $dG(x)/dx$.

An approximation to integral 4.25 can be found by expanding $F(x)$ about x = 0. The integral can further be rewritten as

$$K_2(\omega) = -\frac{2}{\pi}\sum_{n=0}^{\infty} \frac{F^{2n}(0)}{(2n)!}\int_0^{\infty} x^{2n} \ln\coth\left(\frac{|x|}{2}\right) dx , \qquad (4.26)$$

because the function $\ln\coth(|x|/2)$ is even and the odd powers of x in the expansion vanish. The $F^{2n}(0)$ term in equation 4.26 corresponds to the 2*n*th derivative of $F(x)$ evaluated at x=0.

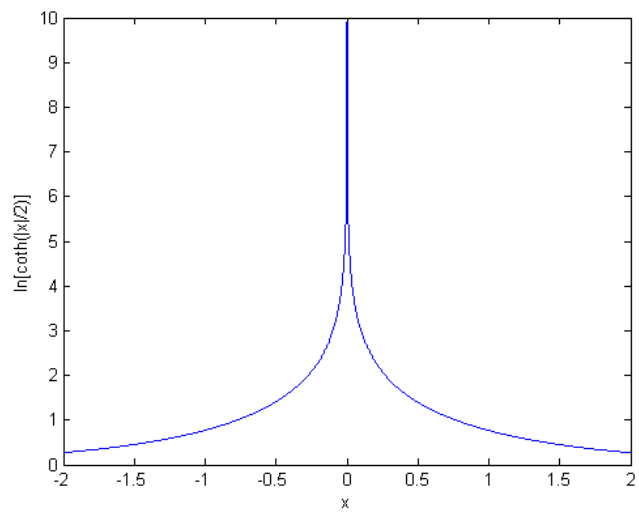

Figure 4.3. The singularity about x=0 for the function ln[coth(|x|/2)]

The next step of the derivation is expanding $\ln\coth(|x|/2)$ in powers of e^{-x} to obtain

$$K_2(\omega) = -\frac{4}{\pi}\left[\sum_{n=0}^{\infty} F^{2n}(0)\left(\sum_{n=0}^{\infty}\frac{1}{(2m+1)^{2n+2}}\right)\right]. \qquad (4.27)$$

This expression shows how K_2 is related to the sum of the even derivatives of $F(x)$ evaluated at x = 0. So long as both the phase velocity and attenuation coefficients are slowly varying in terms of frequency, the equation 4.27 can be approximated by the first few terms. Equations 4.28 and 4.29 represent the equation in 4.27 under these conditions.

$$K_2(\omega) = -\frac{4}{\pi}\left(\frac{\pi^2}{8}F(0) + \frac{\pi^4}{96}F''(0) + \cdots\right) \qquad (4.28)$$

Substituting for $F(x)$ yields

$$K_2(\omega) = -\frac{\pi}{2}\frac{dG(x)}{dx}\bigg|_{x=0} - \frac{\pi^3}{24}\frac{d^3G(x)}{dx^3}\bigg|_{x=0} + \cdots \qquad (4.29)$$

The component $dG(x)/dx$ is related to the dispersion, $dC(\omega)/d\omega$, and evidence to this will be provided below. The higher derivatives of G(x) also correspond to the higher derivatives of the phase velocity in the frequency domain. As long as the change of dispersion is small over a limited frequency range, the higher order derivatives can be neglected. When the first order derivative dominates, the higher order terms can be neglected and the leading term in equation 4.29 can be written as

$$\frac{dG}{dx}\bigg|_{x=0} = \frac{dK_1(\omega)}{d\omega}\frac{d\omega}{dx}\bigg|_{x=0} = \omega\frac{dK_1(\omega)}{d\omega}, \qquad (4.30)$$

and $K_2(\omega)$ becomes

$$K_2(\omega) = -\frac{\pi}{2}\omega\frac{dK_1(\omega)}{d\omega}. \qquad (4.31)$$

This last equation relates the imaginary component of the compressibility at a given frequency to the local rate of change of the real component at the same frequency. Looking at equation 4.21, which relates the phase velocity to the real component of the compressibility, the derivative of $K_1(\omega)$ in the frequency domain becomes

$$\frac{dK_1(\omega)}{d\omega} = -\frac{2}{\rho_0 C^3(\omega)}\frac{dC(\omega)}{d\omega} \qquad (4.32)$$

Now equation 4.32 can be combined with equation 4.31 and 4.22 so that $dC(\omega)/d\omega$ becomes

$$\frac{dC(\omega)}{d\omega} = 2C^2(\omega)\alpha(\omega)/\pi\omega^2, \qquad (4.33)$$

and $\alpha(\omega)$ becomes

$$\alpha(\omega) = \frac{\pi\omega^2}{2C^2(\omega)} \frac{dC(\omega)}{d\omega}. \tag{4.34}$$

Equation (4.33) can be rewritten as

$$\frac{dC(\omega)}{C^2(\omega)} = \frac{2\alpha(\omega)}{\omega^2} d\omega, \tag{4.35}$$

in order to integrate both sides from some reference frequency ω_0 to ω. By doing this, the phase velocity can be related to the attenuation coefficient according to the expression

$$\frac{1}{C_0} - \frac{1}{C(\omega)} = \frac{2}{\pi} \int_{\omega_0}^{\omega} \frac{\alpha(\omega')}{\omega'^2} d\omega', \tag{4.36}$$

where C_0 is the sound velocity at ω_0. Equations 4.34 and 4.36 represent nearly localized approximations relating the attenuation coefficient and the phase velocity. The magnitude of the dispersion is usually small; therefore these equations can be further simplified to

$$\alpha(\omega) = \frac{\pi\omega^2}{2C_0^2} \frac{dC(\omega)}{d\omega}, \tag{4.37}$$

$$\Delta C = C(\omega) - C_0 = \frac{2C_0^2}{\pi} \int_{\omega_0}^{\omega} \frac{\alpha(\omega')}{\omega'^2} d\omega' \tag{4.38}$$

where $C(\omega)$ is written as $C_0 + \Delta C(\omega)$ with $\Delta C(\omega) << C_0$, and only terms of order $\Delta C(\omega)$ are retained. For calculations used in this experiment, equation 4.37 is the only necessary approximation needed. Equation 4.37 is applied to each point of the dispersion curve generated by the laser probe data in order to generate an attenuation coefficient curve over the same range of frequencies. This attenuation curve can then be used in conjunction with the dispersion to calculate Material Q as seen in equation 1.2.

CHAPTER 5

EXPERIMENTAL PROCEDURE

This chapter will outline the experimental method I have developed to measure material Q over frequency. The first section will discuss the preparation of the wafer and the laser probe so that acoustic data can be measured by the probe. The second section walks through how to acquire data using the laser probe and describes how the dispersion curve acquisition software works. The last section will present the software I have written along with Ryan Westafer, to extract the necessary data from the measured waveforms. It will also discuss the other software program I have written which applies the Kramers-Kronig approximations to calculate the attenuation and ultimately material Q.

5.1 Experimental Preparation

Once a material is selected to be characterized by the laser probe, preparation of the material for excitation beam absorption is essential. If the absorption spectrum of the material is known to be very strong for 532 nm green light, no extra preparation is needed. If the test material poorly absorbs 532 nm light a thin layer of copper should be evaporated onto the surface of the wafer. The thickness of the copper should be something that is acoustically thin enough to have a minimal effect on the Rayleigh waves of the substrate, yet optically thick enough to absorb a significant amount of green light to generate a thermal grating. We have found ~100 nm of copper to be a suitable thickness. Once the copper layer is evaporated on the surface of the test material, the material should be lined up on the aluminum plate. The aluminum plate is 8.5 inches in diameter and has straight lines etched perpendicular to each other. These lines are used to line up the flats of a wafer in a given direction so the experimenter has more precise

control over the wave propagation direction. Below where the wafer sits, angles are labeled, ranging from negative 45 degrees to positive 45 degrees. Four notches were made into the side of the plate so the experimenter could line up the lines on the plate with the angles labeled on the side of the motor stage. Figure 5.1 is a diagram of what the aluminum plate looks like. Figure 5.2 shows the aluminum plate aligned with the angle strip on the side of the wafer stage.

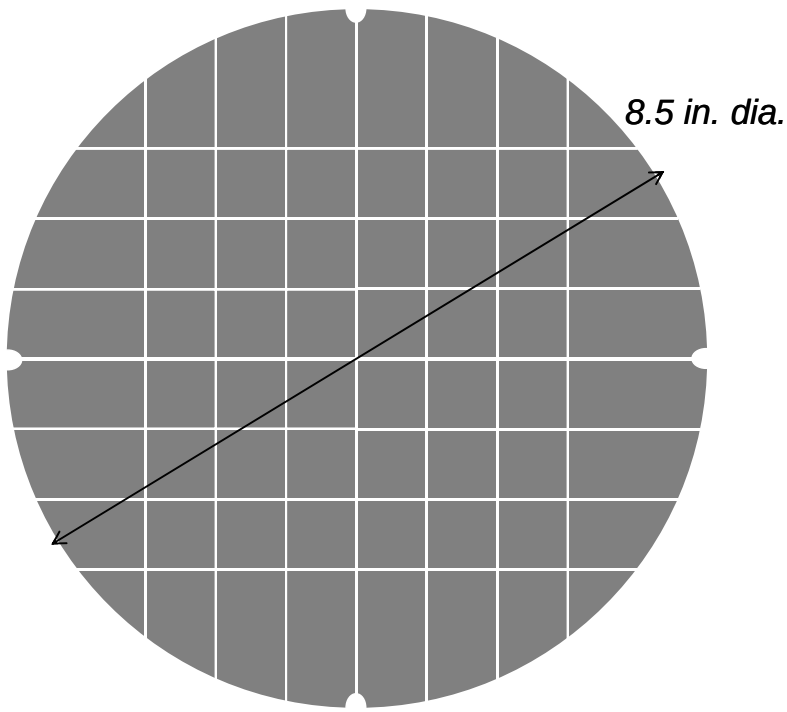

Figure 5.1. The aluminum plate used to align the direction of the test wafers with the desired direction of the acoustic wave

Figure 5.2. The angles labeled from -45 to +45 degrees on the side of the wafer stage.

Once the wafer is in place it is ok to turn on the system. However, before turning on the system it is essential protective eye wear is worn to prevent eye damage from the laser beams. Of the two lasers used, it is better to use eye protection designed for infrared light. The visible green light can trigger the natural human reaction to look away from an intense light source. While not visible to the human eye, the infrared light is still intense enough to damage eyesight. With no ability for the human eye to react and look away from invisible light, the infrared light poses a greater threat to the experimenter. Turning on the system is done by making sure the amplifiers for the motors, the power supply for the photoreceiver, and the Nanolase power supply for the excitation and probe lasers are all turned on. Once the system is online it is ok to run the GUI software for the laser probe.

After the software has finished homing the motors, finite alignment is then required of the motor stage. Each test sample may be of a different thickness therefore it is possible the target may be misaligned in the vertical direction. If the target is misaligned the two excitation beams and probe beam will not be coincident on the sample and little or no signal will be visible on the oscilloscope. To align the system, simply fire the laser while adjusting the height of the stage until the waveform on the oscilloscope is maximized. Figure 5.3 shows the laser arrangement depending on the height of the wafer.

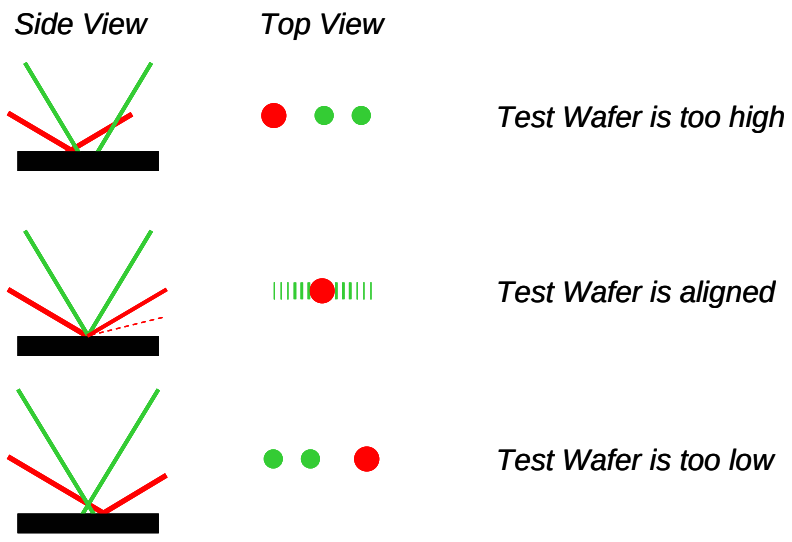

Figure 5.3. The excitation (green) and probe (red) laser beam arrangement depending on alignment

Once the signal is maximized it then becomes necessary to determine which NDF setting the excitation beam should pass through to ensure the metal does not melt during the experiment. If the setting is not already known this information can be found empirically by targeting a “scrap” area of the surface and increasing the NDF setting until the metal begins to melt. One can tell if the metal is melting, if the oscilloscope signal begins to become deformed or if there is exceptional scattering of the target spot on the camera view. Before and after images of the waveform and scattered light off the melted metal can be seen in Appendix B.

At this point, the experimenter must then input the wavelengths that are used for the dispersion curve by selecting the phase mask settings that correspond to the desired wavelengths. Table 5.1 shows the wavelengths generated by each phase mask. To input the phase masks for the program to use, enter each one into the array box next to the

dispersion curve “Go” button. In order for the MATLAB software to interpolate properly, at least nine phase masks should be selected prior running the program.

Table 5.1. Corresponding wavelength values for each phase mask

Phase Mask Number	Wavelength (microns)	Phase Mask Number	Wavelength (microns)
1	60	13*	9.43
2	50	14*	8.825
3	30	15*	8.23
4	25	16*	7.755
5*	20.75	17*	7.25
6*	17.15	18	6.5
7*	14.1571	19	6.0
8*	12.3875	20	5.5
9*	11.333	21	5.0
10*	10.8625	22	4.0
11*	10.2875	23	3.0
12*	9.71	24	5.25 (3-beam)

* determined by SEM imaging on an interference pattern burnt spot

5.2 Acoustic Data Acquisition

Once these steps have been completed the user is then ready to collect dispersion data. The program itself takes less than 1 minute to collect data and the mathematical analysis of the data is also very quick and finishes in a matter of seconds. The program starts by aligning the first selected phase mask into the path of the excitation beam and the laser is turned on. The oscilloscope is then cleared from any previous data and the math settings are set up to average the data for 500 sweeps. Averaging the signal is necessary to remove any noise that may randomly occur during a single sweep of the signal. Once the data is collected, the laser is turned off and the next phase mask is selected. Every iteration takes roughly two seconds to complete and another half second to move between phase masks, resulting in 2.5 seconds between every cycle. The waveforms are collected as a time array and an amplitude array. On a time scale of 20 ns with a sampling rate of 2 Giga-samples/second a total of 401 data points are generated

per waveform. These arrays are then appended to the data matrix where each odd column is a time array and each even column is the corresponding amplitude array. A header row is also included to distinguish which column corresponds to which phase mask. Once all the phase masks have been visited by the optics head the file is saved as a text file that can be opened by MATLAB.

5.3 Mathematical Analysis Software

Appendix A includes the m-files used in analyzing the data matrix created by the dispersion curve program from the previous section along with a sample data matrix file. When the file DispersionCurves.m is run within MATLAB, the program first asks to load a data matrix file so that it can extract each individual waveform. The header row of the data matrix is used to keep track of which phase mask goes with which waveform. An example of the data matrix is included in Appendix A as well. Next, the software reads the header and uses the data seen in table 5.1 to assign a wavelength value to each waveform. Each waveform is then individually analyzed to determine the frequency of the acoustic wave measured. In order to analyze the frequency spectrum of the waveform the thermal decay component of the data must be removed to eliminate the low frequency content generated by the decay. This is done by using the decimate function in MATLAB. The decimate function acts as an eighth order Chebyshev low pass filter and filters the frequency content below the specified cut off frequency. This program defaults to a 300 MHz cut off frequency which is suitable for most waveform measured on most materials. If the center frequency of the acoustic content of a waveform is less than or equal to 300 MHz, a lower cut off frequency can be entered to preserve accuracy. Figure 5.4 represents a waveform of a 10.5 micron surface acoustic wave on a silicon substrate with

100 nm of copper evaporated on top. Plot A represents the initial waveform before any filtering. Plot B represents the time signal after low pass filtering at 150 MHz. Lastly, Plot C represents the “cleaned up” time domain waveform after filtering.

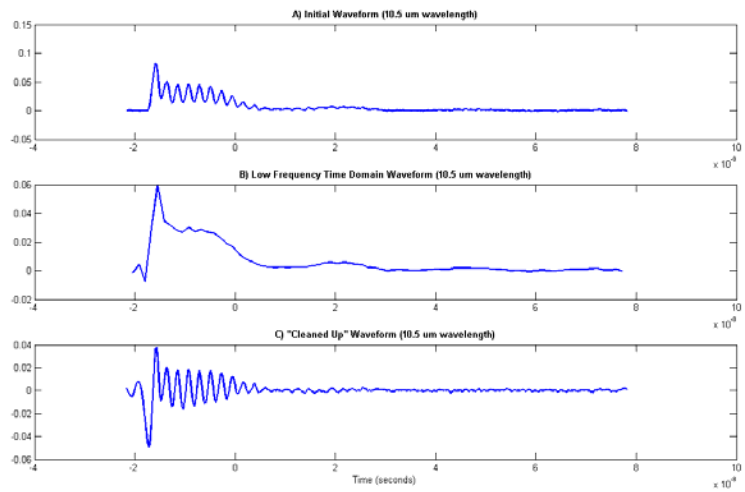

Figure 5.4. (Prefiltered signal A) – (150 MHz Low Pass Filtered B) = (150 MHz High Pass filtered C)

Once the waveform is cleaned up, a FFT is performed on the clean waveform. The waveform is zero-padded ten fold to improve the resolution of the frequency domain. The software then searches the remaining data for the maximum point of the spike in the frequency domain such as the one in figure 5.5.

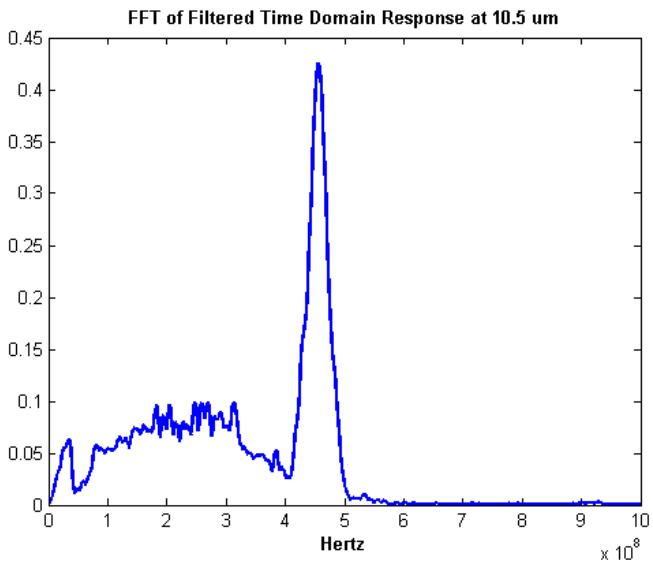

Figure 5.5. FFT the cleaned up waveform from Figure 5.7 C

Once each waveform's frequency has been determined, it is then possible to calculate the phase velocity of the wave using the known wavelengths. A dispersion curve over frequency can then be generated knowing each waveforms velocity and frequency. The software program then applies the Kramers-Kronig approximation to go from the dispersion curve to the values for the attenuation coefficients. Equation 4.37 from chapter four is used to attain the attenuation coefficients. Next, the attenuation coefficients are converted to Nepers/meter so the values can be used to calculate Material Q. The equation for material Q (equation 1.2) is then applied using the attenuation and dispersion data to generate values. Finally, the software program plots the three curves for dispersion, attenuation, and Material Q all over frequency. An example of these plots will be shown in the next chapter regarding the analysis of the experimentally measured data.

CHAPTER 6

ANALYSIS OF RESULTS

The purpose of this chapter is to provide results measured by the experimental technique outlined in this thesis. We evaporated 100 nm of copper onto the surface of a silicon wafer and took measurements in the (100) direction and 30 degrees off of (100). The Microwave Acoustics Handbook by A.J. Slobodnik et al. [17] define the nominal Rayleigh wave velocities of 100 cut Silicon and isotropic copper as 5.032 km/s and 2.235 km/s respectively. Noting that the copper surface layer has a much slower velocity than the substrate, it stands to reason that the Rayleigh velocity will actually decrease as the wavelength decreases because more of the acoustic energy is in the surface film. Due to this, an increase in frequency will also result in a decrease in velocity as a higher percentage of the surface wave propagates within the surface layer. This decrease in velocity as frequency increases for this particular range is observable in both the theoretical data as well as the experimental data. The theoretical data was generated using an FDTD (Finite Difference Time Domain) simulation program written and developed by Saeed Mohammadi at Georgia Tech. Both the experimental data as well as the theoretically calculated data for the dispersion, attenuation, and material Q will be presented in this chapter.

Before comparing the data acquired by the laser probe to the theoretically determined data I would like to quickly discuss the FDTD method used in this experiment. The strength of the FDTD method is the ability to characterize wave propagation in non-uniform and nonlinear media. This numerical technique was first pioneered by K. S. Yee in 1966 in order to discretize the differential form of Maxwell's

equations[18]. He used an electric-field grid that was offset both spatially and temporally from a magnetic field grid. This was done in order to have update equations that yield the present fields throughout the computational domain in terms of the past fields. These update equations for the electric and magnetic fields were used in a leap frog manner to calculate the fields in the time domain. While the FDTD method has been around since the sixties, it has only been since the advent of today's computing power that engineers and scientists have been able to fully take advantage of this technique. PC clusters are often used to take advantage of the parallelism in the FDTD method and to minimize the time to run the simulation [18, 19]. The FDTD technique has also been utilized in the field of acoustics especially in the study of phononic crystals.[20] While the FDTD used in my experiment was originally designed for acoustic wave propagation in periodic lattices, it proved to be more than sufficiently designed to study bi-layered media.

6.1. Experimental vs. Theoretical Data

The experimental data measured in this experiment was collected from a p-doped 100 cut silicon wafer with 100 nm of copper evaporated onto the surface. The wafer was oriented on the laser probe stage so the generated wave would propagate in the 100 direction. Phase masks 9-17 were used in the dispersion curve software program which give a wavelength range of 7.25 um to 11.333 um. Very little is published with regards to Rayleigh wave material Q values and therefore there is no data available in literature to compare my results. However, because the Kramers-Kronig relations for acoustic waves have been verified by various sources [5, 6, 15], the need for preexisting Q values is no longer necessary. I have, however, provided theoretical dispersion data generated by the FDTD method to compare my experimental data to what can be predicted. Due to the

intense processing time necessary for the FDTD method to calculate a dispersion curve with a high enough frequency resolution, an alternative approach was used. The FDTD method was run over a wavelength range of .8 um all the way up to 160 um for about 15 points and the data was interpolated. The calculation of these 15 points took over a day to calculate on one computer. I now present the Dispersion data measured by the laser probe with the corresponding theoretical data calculated by the FDTD method over the range of interest.

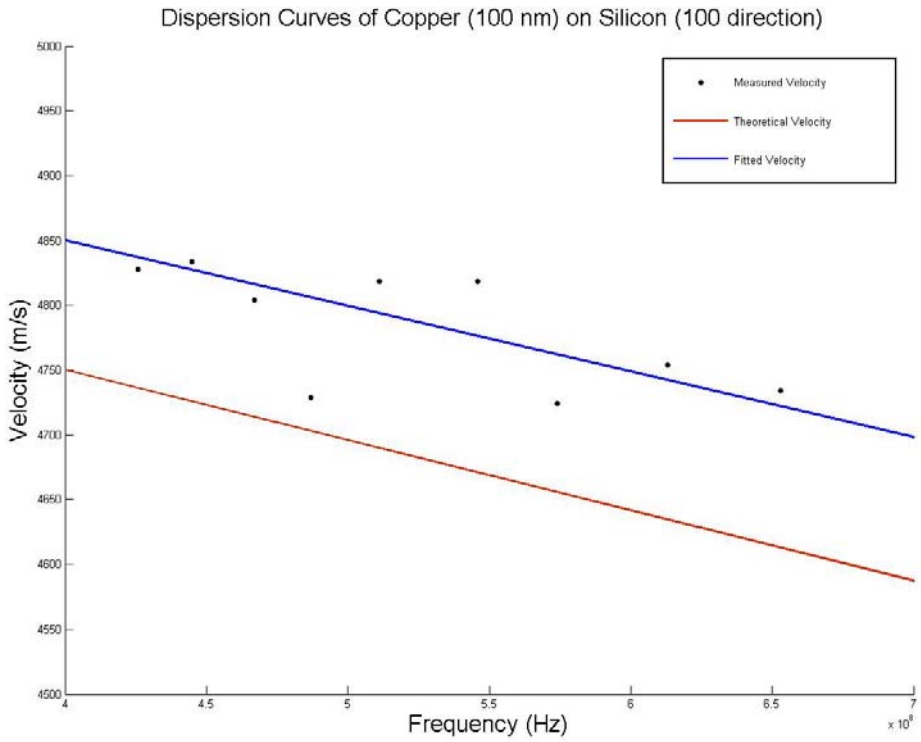

Figure 6.1. Theoretical (red) and experimental (blue) results for 100 nm of copper on Silicon in the (100) direction

Figure 6.1 shows the velocity measured by the laser probe. A linear fit was done to the points to better show the trend of the velocity as frequency increases. The red line in the plot represents the theoretically determined data. The two lines differ by only about

2.5% and both share the same downward trend as frequency increases. This negative slope counters the typical dispersion trend of the velocity increasing over frequency. The velocities decrease as frequency increases because the surface copper layer has a much slower velocity than the bulk silicon (2.235 km/s vs. 5.032 km/s). As the frequency increases and the wavelength decreases, a greater percentage of the Rayleigh wave exists in the surface layer. As a result the velocity will decrease until the wavelength of the surface wave is less than thickness of the top layer.

As previously mentioned in chapter five, once the dispersion data is measured, the attenuation coefficients can then be calculated using the Kramers-Kronig approximations for a local dataset. Figure 6.2 is the plot of the calculated attenuations coefficients for both the experimental and theoretical data.

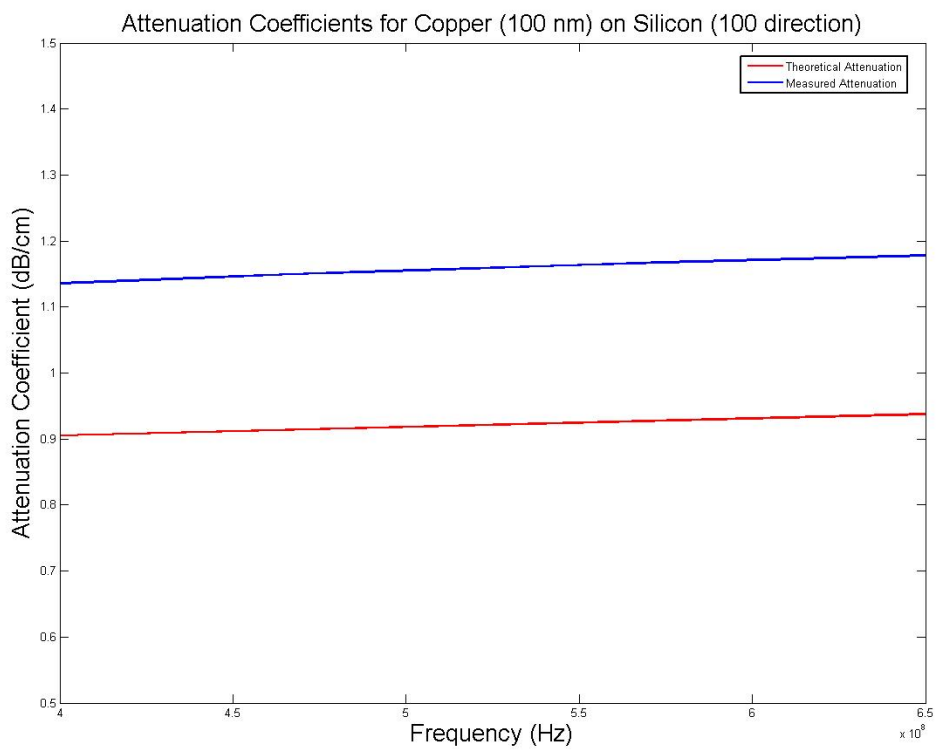

Figure 6.2. Calculated Attenuation Coefficients for the Theoretical (red) and Experimental (blue) data using the Kramers-Kronig approximations for local data

Unlike the dispersion data, the attenuation data shows a trend that coincides more with the common notion that the attenuation of a wave increases as the frequency increases. It is also worth noting that the measured attenuation is greater than the theoretical attenuation. This is due to the losses in the material that can not be accounted for in the FDTD simulation.

Having both the attenuation data and the dispersion data known for a range of frequencies, the final step to calculate Material Q can be taken. Figure 6.3 shows the final material Q values for the FDTD simulated data and the experimentally measured data from the laser probe.

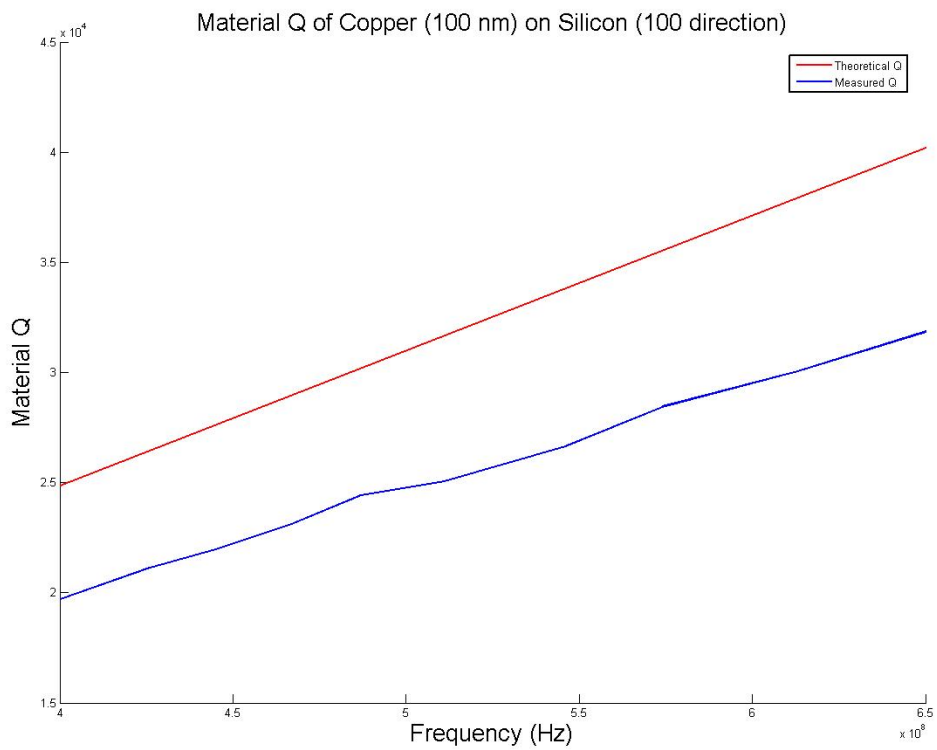

Figure 6.3. The measured Material Q for both the FDTD simulated data (red) as well as the experimentally measured laser probe data (blue)

The data provided here shows the Material Q for this local frequency range on the order of 10^4. Like the dispersion curve, this particular range of frequencies does not exhibit the correct trend as frequency increases. This once again has to do with the fact that the top layer becomes a factor as the wavelengths decrease. From this data it becomes clear that as the wavelength gets shorter and a higher percentage of the surface wave exists in the top layer, the acoustic energy propagates more efficiently within the material. The material Q values calculated from the theoretical data are higher and appear more efficient than the experimentally determined material Q values. This once again stems from the inability for the FDTD software to account for all loss mechanisms that maybe be occurring as the wave propagates.

6.2. Material Q over Direction

This next section will present two extra sets of Material Q calculations for the same physical arrangement of copper evaporated on silicon that was seen in the previous section. Figures 6.4 and 6.5 show the measured data of the test structure in the (100) direction and 30 degrees off the (100) direction. Figure 6.4 clearly shows a phase velocity range beginning at 4.9 km/s and ending around 4.75 km/s. The material Q for this direction begins at 20,000 and ends around 37,500. Figure 6.5 shows a slightly faster velocity beginning just under 5 km/s and ending just above 4.8 km/s. The attenuation data for this direction also appears marginally higher than that of the (100) direction. As a result the material Q is slightly lower starting at just under 20,000 and finishing right around 35,000 at 650 MHz. This shows that if both the attenuation coefficient and dispersion curves are greater in magnitude a lower Q value will be determined.

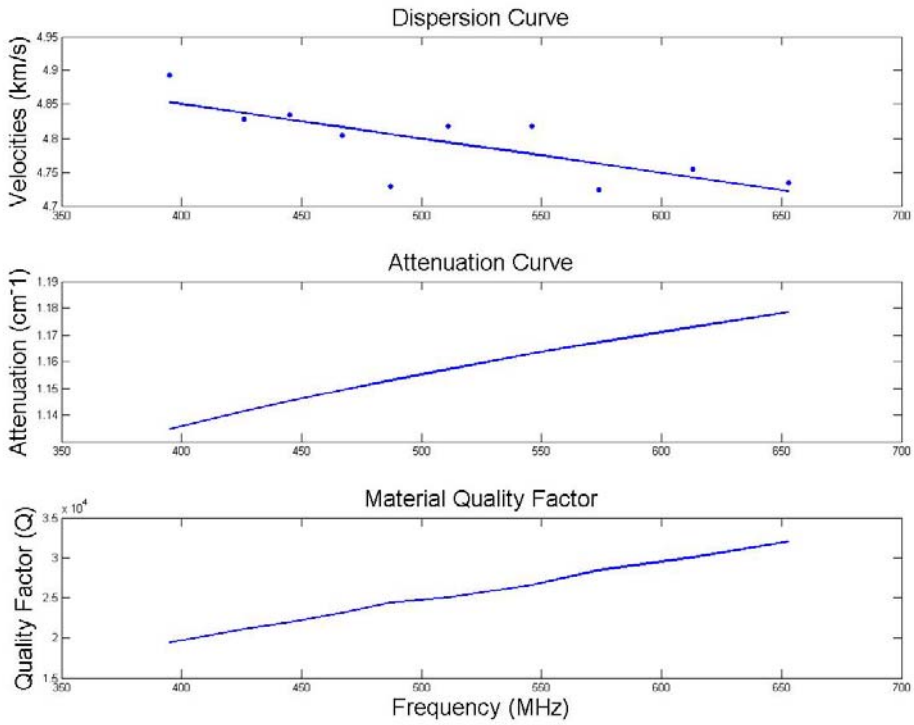

Figure 6.4. Measured data in the (100) direction

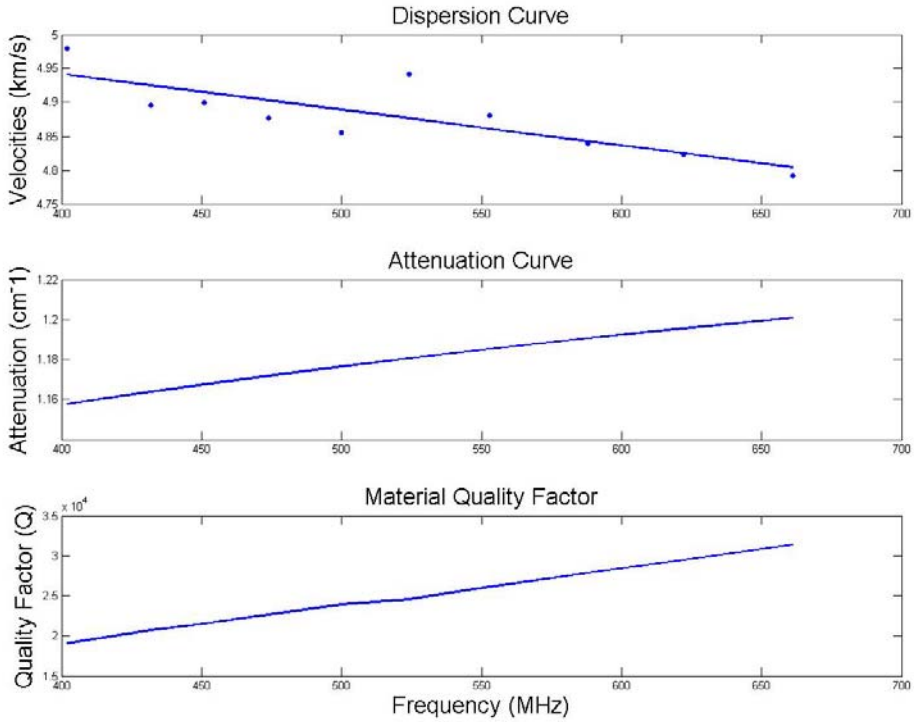

Figure 6.5. Measured data 30 degrees from the (100) direction

CHAPTER 7

CONCLUSION

In this thesis, I have demonstrated a non invasive means of measuring the Rayleigh wave Q for a given material with a laser probe. The probe itself relies on the transient grating method to generate Rayleigh waves on the surface using a series of binary phase masks. While the optics head was originally designed to measure ultra thin film metal thicknesses for CMOS circuits, we have found another way to interpret the data to suit our needs. We have written our own programs to automate the laser probe and measure the frequency of waves generated by a range of phase masks. Knowing the wavelength of the generated acoustic wave and after the frequency of the wave is determined, the phase velocity for each wave can be calculated and dispersion data for a range of ultrasonic becomes known. In order to generate the attenuation data needed for the calculation of material Q, a local approximation of the Kramers-Kronig relations that was developed by M. O'Donnell et al. [5] is used. The Kramers-Kronig relations for acoustic waves relate the real and imaginary parts of the dynamic compressibility for a material. While the real part of the compressibility relates to the velocity, the imaginary part can be related to the attenuation. Given both the attenuation and dispersion, material Q can easily be calculated for surface waves of the given sample. The results chapter of this thesis shows measurements I have taken and discusses the behavior of dispersion, attenuation, and material Q curves. Since very little is found in literature regarding the Rayleigh Wave Q values for different materials, the need for rapid measurement can be found useful. In summation, my technique has demonstrated the ability to quickly measure material Q while remaining minimally invasive to the test structure.

APPENDIX A

MATLAB CODE USED FOR ANALYSIS OF DISPERSION DATA

```
function [Q,Attenuations,Frequencies,Wavelengths,Velocities] =
DispersionCurves(varargin)
% DispersionCurves; allows the user to open a Dispersion Data file
% generated by the laser probe and calculate material Q
%
% DispersionCurves('Plot') allows the user to also plot every waveform that
% was acquired by the laser probe
% By Eric Massey 2006

% determine whether or not to plot each waveform
if isempty(varargin)
   Plot='no';
else
   Plot=cell2mat(varargin(1));
end

% import the file with the different waveforms
S=uiimport('-file');

% get the names of each waveform
Names=S.colheaders;

% from the names retrieve the values of the phase masks used
PM=zeros(1,length(Names));
for I = 1:length(Names)
   PM(I)=sscanf(char(Names(I)), 'PM%d');
end
PM=downsample(PM,2); % this was done b/c each phase mask was listed twice


% Here are the wavelengths that correspond to each phase mask
PMIndex=[60.0 50.0 30.0 25.0 20.0 17.0 14.0 12.0 11.0 10.5 10.0 9.5 9.0 8.5 8.0 7.5
7.0 6.5 6.0 5.5 5.0 4.0 3.0 5.25];
```

A.1. Matlab code for the function DispersionCurves.m

```
% SEM images were done on burnt scrap test pieces to determine the
% wavelengths of each phase mask...these are the SEM values
PMIndex(19)=12/2;
PMIndex(18)=13/2;
PMIndex(17)=7.25;
PMIndex(16)=15.51/2;
PMIndex(15)=8.23;
PMIndex(14)=8.825;
PMIndex(13)=9.43;
PMIndex(12)=9.71;
PMIndex(11)=10.2875;
PMIndex(10)=10.8625;
PMIndex(9)=11.3333;
PMIndex(8)=12.3875;
PMIndex(7)=14.1571;
PMIndex(6)=17.15;
PMIndex(5)=20.75;
PMIndex=PMIndex.*1e-6; % convert all wavelengths to microns

% prepare the Wavelengths array
WAVELENGTHS=zeros(1,length(PM));

% create an array with all the wavelengths used by the laser probe
for I = 1:length(PM)
   WAVELENGTHS(I)=PMIndex(PM(I));
end

% the cut off freq used by the program WaveData.m to clean up the waveform
CutOffFreq=300000000;

% prepare the Velocities array
Velocities=zeros(1,length(WAVELENGTHS));

% Extract each waveform array (time,amp) and send it to WaveData.m for
% analysis. For each waveform the wavelength (already known), frequency
% and velocity can be learned
for I = 1:length(WAVELENGTHS)
   D(:,1)=S.data(:,2*I-1);    % D(:,1) is the time column
   D(:,2)=S.data(:,2*I);    % D(:,2) is the Amp column
   [Freq Wavelength Velocity]=WaveData(D,WAVELENGTHS(I),CutOffFreq,Plot);
   Velocities(I)=Velocity;
   Frequencies(I)=Freq;
   Wavelengths(I)=Wavelength;
end
```

A.1. Matlab code for the function DispersionCurves.m (cont.)

```
% convert from Hz to radians
Omegas0=Frequencies.*2.*pi;

% smooth the velocity data to find the derivitive
ftype=fittype('smoothingspline');
fit1=fit(Frequencies',Velocities',ftype);
VelCol=Velocities';
Vdiff=differentiate(fit1,VelCol);
% This is eqation 30a from O'Donnell et al:
% Relation between attenuation and velocity
% J. Acoust. Soc. Am.,Vol.69,No.3, March 1981
Attenuations=(pi.*Omegas0.^2/(2*Velocities(1))).*Vdiff'


Att=10*log10(Attenuations); % convert to decibels/m
Attenuations=Att./100;            %convert to db/cm
Np=Att./8.7; % convert to Np/m
Q=Omegas0./(2.*Velocities.*Np); % Find Q factor

% This code is redundant and was done a second time as well and redundant
Velocities=Velocities
Frequencies=Frequencies
Wavelengths=Wavelengths
Attenuations=Attenuations
Q=Q

% Plot that SOB!
figure
hold off;
cla;
subplot(3,1,1);
plot(Frequencies./1e6,Velocities./1e3);
title('Dispersion Curve');
ylabel('Velocities (km/s)');
subplot(3,1,2);
plot(Frequencies./1e6,Attenuations);
title('Attenuation Curve');
ylabel('Attenuation (cm^-1)');
subplot(3,1,3);
plot(Frequencies./1e6,Q);
title('Material Quality Factor');
ylabel('Quality Factor (Q)');
xlabel('Frequency (MHz)');
```

A.1. Matlab code for the function DispersionCurves.m (cont.)

```
function [varargout] = WaveData(varargin)
% []=WaveData(Waveform), This will just plot the waveform and an fft
%
% [Frequency,Wavelength,Velocity]=WaveData(Waveform,Wavelength)
% input the wavelength of the waveform and the waveform itself to get the
% output variables
%
% [Frequency,Wavelength,Velocity]=WaveData(Waveform,Wavelength,Plot)
% input the wavelength of the waveform and the waveform itself to get the
% output variables, Plot must be = to 'Plot' to plot the waveform
%
% [Frequency,Wavelength,Velocity]=WaveData(Waveform,Wavelength,CutOffFreq)
% input the wavelength of the waveform and the waveform itself to get the
% output variables, CutOffFreq filters out all the junk below that
% frequency
%
%
[Frequency,Wavelength,Velocity]=WaveData(Waveform,Wavelength,CutOffFreq,Plo
t)
% input the wavelength of the waveform and the waveform itself to get the
% output variables, Plot must be = to 'Plot' to plot the waveform
% By Eric Massey, edited by Ryan Westafer 2006


% This block of code determines which variables have been entered into the
% function
Waveform=cell2mat(varargin(1));
if length(varargin)==1
   plotme=1;
   Wavelength=0;
   CutFF=0;
   outvars=0;
elseif length(varargin)==2
   plotme=0;
   Wavelength=cell2mat(varargin(2));
   CutFF=0;
   outvars=3;
elseif length(varargin)==3
   if ischar(cell2mat(varargin(3)))
      plotme=1;
      Wavelength=cell2mat(varargin(2));
      CutFF=0;
      outvars=3;
```

A.2. Matlab code for the function WaveData.m

```
   else
      plotme=0;
      Wavelength=cell2mat(varargin(2));
      CutFF=cell2mat(varargin(3));
      outvars=3;
   end
else
   if strcmp(cell2mat(varargin(4)),'Plot')
      plotme=1;
   else
      plotme=0;
   end
   Wavelength=cell2mat(varargin(2));
   CutFF=cell2mat(varargin(3));
   outvars=3;
end
%%%%%%%%%%%%%%%%%%%%%%%%%%%%%%%%%%%%%%%%%
%%%

% Time data sampling frequency
Fs=2e9;  % 2GHz

% Set up the time data to start at t = 0
TimeIn=Waveform(:,1);
AmplitudeIn=Waveform(:,2);

% Make vector with first time point == 0
if TimeIn(1) ~= 0
   Time0=TimeIn-TimeIn(1);
else
   Time0=TimeIn;
end

% Define MeasurementDuration
MeasurementDuration = Time0(end);

% Get time indices from t==0 up to t==MeasurementDuration
TimeStop = find(Time0>=MeasurementDuration,1);
% Truncate Time and Amplitude accordingly
Time = Time0(1:TimeStop);
Amp = AmplitudeIn(1:TimeStop);
```

A.2. Matlab code for the function WaveData.m (cont.)

```
% Do Low-pass Filtering?
if CutFF ~= 0
   % do low-pass filter
   % Compute R according to 'doc decimate'
   R=fix(.8*(Fs/2)/CutFF);
   % down-sample to throw out high frequencies
   DecimatedAmp=decimate(Amp,R);
%     figure;
% %     subplot(3,1,1);
%     plot(TimeIn,Amp);
   % up-sample to original rate w/ only low freq. remaining
   LowPassedAmp=interp(DecimatedAmp,R);
   % subtract off low-frequency time signal
   NewAmp = Amp - LowPassedAmp;

else
   % Do nothing
   NewAmp = Amp;
end


% DO ZERO-PADDED FFT
ZPad=10;
% Set # of points for fft to be ZPad * original#
ZPadLength=ZPad*length(NewAmp);
FFTAmp=fft(NewAmp,ZPadLength);

% Power spectrum, don't care to normalize by # points
PP=FFTAmp.*conj(FFTAmp);
% frequency starts at zero, so subtract 1
% divide by padding length (#PadPoints)
% to get back to original #points
f=(2*Fs) * (1-1:length(PP)-1)/ZPadLength;
% only take lower symmetric half
halff = fix(length(f))/2;
% only take up to Fs/2
Fs2 = halff/2;
% truncate frequency and power spectrum
f=f(1:Fs2);
P=PP(1:Fs2);
% find frequencies above cutF
cutF=find(f>=CutFF,1);
```

A.2. Matlab code for the function WaveData.m (cont.)

```
% The wavelength can be entered in terms of MHz or Hz, however the
% frequency scale is always MHz
% i.e. Wavelength = 200 --> 200 MHz
%  or  Wavelength = 200e6 --> 200 MHz
% this block allows for that
if Wavelength>1e-3
   Wavelength=Wavelength*1e-6;
end

% if plot was selected then plot the waveform
if plotme
   figure;
   plot(f,P);
   title(sprintf('FFT of Filtered Time Domain Response at %g
um',Wavelength*1e6));
   xlabel('Hertz');
end


% find the center frequency of the "cleaned" up waveform
Frequency=f(find(P(cutF:end)>=(max(P(cutF:end))),1)+cutF-1);
Velocity=Frequency*Wavelength;

% handle outputs for the function
if outvars==0
   varargout={};
else
   varargout(1)={Frequency};
   varargout(2)={Wavelength};
   varargout(3)={Velocity};
end
```

A.2. Matlab code for the function WaveData.m (cont.)

```
PM8,PM8,PM9,PM9,PM10,PM10,…
-2.162500E-8,0.000525,-2.162500E-8,0.000586,-2.162500E-8,0.000110,…
-2.137500E-8,0.000562,-2.137500E-8,-0.000610,-2.137500E-8,0.000159,…
-2.112500E-8,3.662110E-5,-2.112500E-8,-0.000220,-2.112500E-8,0.000781,…
-2.087500E-8,-1.220703E-5,-2.087500E-8,0.000183,-2.087500E-8,0.000757,…
-2.062500E-8,3.662110E-5,-2.062500E-8,0.000940,-2.062500E-8,9.765625E-5,…
-2.037500E-8,-0.000330,-2.037500E-8,-0.000146,-2.037500E-8,-0.000244,…
-2.012500E-8,-0.000439,-2.012500E-8,0.000220,-2.012500E-8,0.000342,…
-1.987500E-8,-0.000122,-1.987500E-8,-4.882813E-5,-1.987500E-8,0.000293,…
-1.962500E-8,0.000159,-1.962500E-8,0.000513,-1.962500E-8,0.000403,…
-1.937500E-8,-0.001099,-1.937500E-8,0.000525,-1.937500E-8,0.000159,…
.
.
.
.
.
.
.
.
.
```

A.3. An example WaveData file

APPENDIX B

GRAPHICAL USER INTERFACE IMAGES

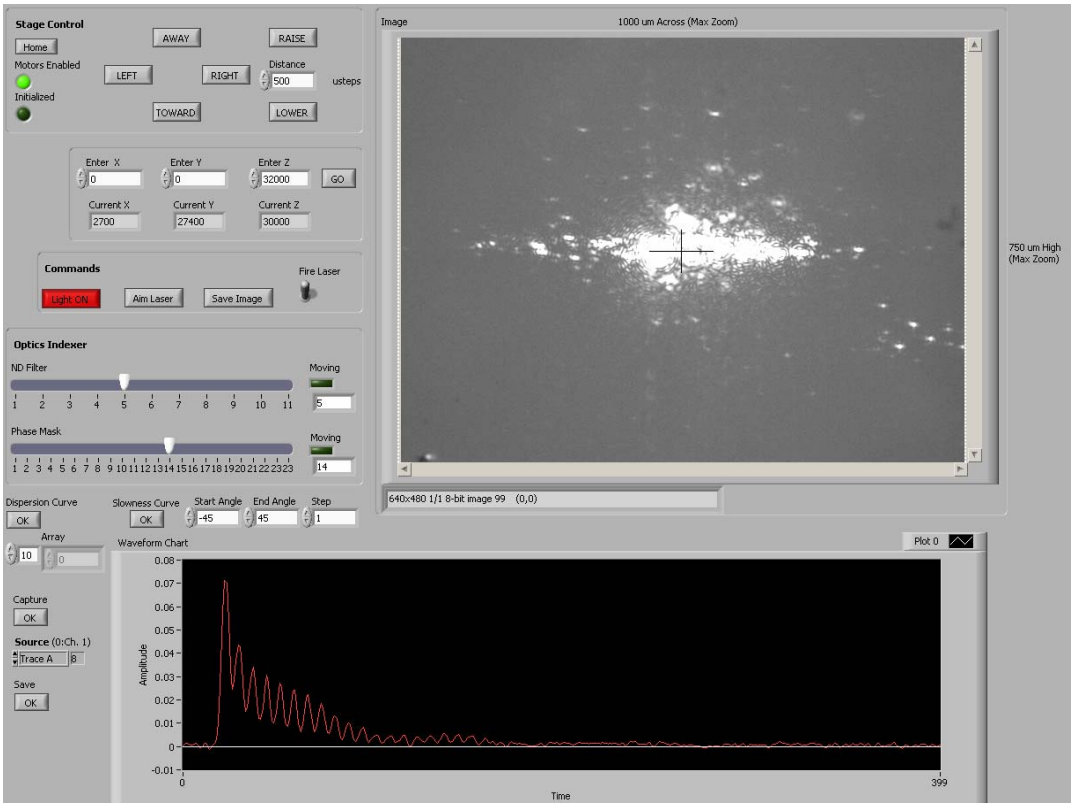

Figure B.1. A strong signal on an NDF setting that isn't destroying the material

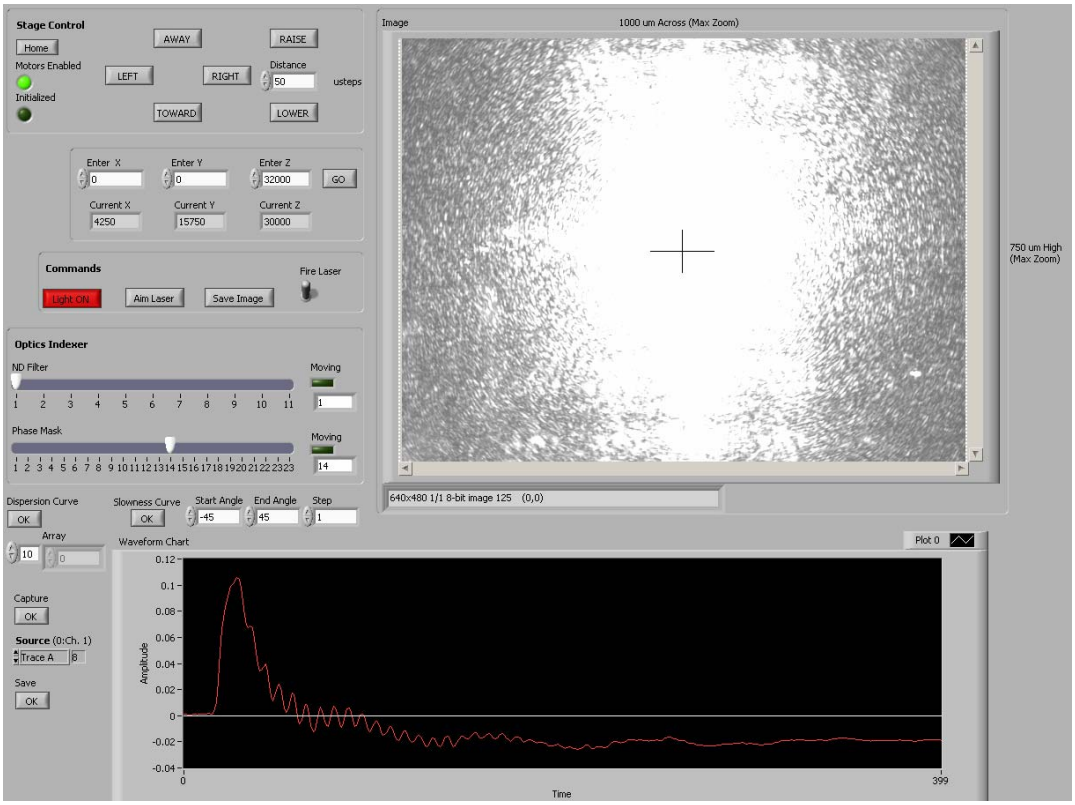

Figure B.1. A deformed signal due to melting of the material

REFERENCES

[1] S. H. Lee, "Theoretical and Experimental Characterization of Time-Dependent Signatures of Acoustic Wave Based Biosensors," in *ECE*. vol. P.h.D Atlanta, GA: Georgia Institute of Technology, 2006.

[2] B. A. Auld, *Acoustic fields and waves in solids*, 2nd ed. Malabar, Fla.: R.E. Krieger, 1990.

[3] J. F. Rosenbaum, *Bulk acoustic wave theory and devices*. Boston: Artech House, 1988.

[4] K. Aki and P. G. Richards, *Quantitative seismology : theory and methods*. San Francisco: W. H. Freeman, 1980.

[5] M. O'Donnell, E. T. Jaynes, and J. G. Miller, "Kramers-Kronig relationship between ultrasonic attenuation and phase velocity," *Journal of the Acoustical Society of America*, vol. 69, pp. 696-701, 1981.

[6] M. O'Donnell, E. T. Jaynes, and J. G. Miller, "General relationships between ultrasonic attenuation and dispersion," *Journal of the Acoustical Society of America*, vol. 63, pp. 1935-7, 1978.

[7] Y. Ebata, "Surface Acoustic Wave Resonator." vol. 4,635,009, U. S. P. a. T. Office, Ed. United States: Kabushiki Kaisha Toshiba 1987.

[8] J. A. Rogers, A. A. Maznev, M. J. Banet, and K. A. Nelson, "OPTICAL GENERATION AND CHARACTERIZATION OF ACOUSTIC WAVES IN THIN FILMS: Fundamentals and Applications." vol. 30, 2000, pp. 117-157.

[9] T. K. Gaylord, "Modulation, Diffractive, and Crystal Optics," 2001.

[10] A. A. Maznev, A. Akthakul, and K. A. Nelson, "Surface acoustic modes in thin films on anisotropic substrates," *Journal of Applied Physics*, vol. 86, pp. 2818-24, 1999.

[11] J. C. Crowhurst, A. F. Goncharov, and J. M. Zaug, "Impulsive stimulated light scattering from opaque materials at high pressure," *Journal of Physics: Condensed Matter*, vol. 16, pp. 1137-42, 2004.

[12] R. d. L. Kronig, "Theory of dispersion of X-rays," *Journal of the Optical Society of America and Review of Scientific Instruments*, vol. 12, pp. 547-557, 1926.

[13] R. L. Kronig and H. A. Kramers, "Absorption and dispersion in x-ray spectra," *Zeitschrift fur Physik*, vol. 48, pp. 174-179, 1928.

[14] P. Bhattacharya, *Semiconductor optoelectronic devices*, 2nd ed. Upper Saddle River, NJ: Prentice Hall, 1997.

[15] C. C. Lee, M. Lahham, and B. G. Martin, "Experimental verification of the Kramers-Kronig relationship for acoustic waves," *IEEE Transactions on Ultrasonics, Ferroelectrics and Frequency Control,* vol. 37, pp. 286-94, 1990.

[16] H. M. Bode, "Relations Between Attenuation and Phase in Feedback Amplifier Design," *Bell System Technical Journal,* vol. 19, 1940.

[17] J. A.J. Slobodnik, E. D. Conway, and R. T. Delmonico, "Microwave Acoustics Handbook." vol. 1A, P. S. R. Papers, Ed.: United States Air Force, 1973.

[18] K. L. Shlager and J. B. Schneider, "A selective survey of the finite-difference time-domain literature," *IEEE Antennas and Propagation Magazine,* vol. 37, pp. 39-57, 1995.

[19] K. Y. Wong and W. Y. Tam, "Analysis of the frequency response of SAW filters using finite-difference time-domain method," Long Beach, CA, USA, 2005, p. 4 pp.

[20] M. M. Sigalas and N. Garcia, "Theoretical study of three dimensional elastic band gaps with the finite-difference time-domain method," *Journal of Applied Physics,* vol. 87, pp. 3122-5, 2000.